Supplementary Note-1. It has been mentioned in the main article that our aim is to understand the loss of H_2SO_4 molecule through its decomposition into various product molecules in presence of $O(^1D)$. For our convenience and to keep the discussion simple, we have referred the insertions/additions of $O(^1D)$ into the O−H, S=O and S−O bonds of H_2SO_4 as the *Channel-I*, *Channel-II* and *Channel-III*, respectively. It is seen from our calculations (see below) that the insertions/additions of $O(^1D)$ through *Channel-I* to *III* produce directly either the adduct intermediates (H_2SO_4−$O(^1D)$ ≡ Ad) or H_2SO_5 in the first step, and once the Ad or H_2SO_5 are formed; they can further undergo unimolecular isomerization or decompositions followed by isomerizations to produce SO_3, H_2O and H_2O_2, as the neutral product molecules and HSO_4 + OH radicals, especially, in presence of sunlight (see Main Article). This is expected because of large exothermicities associated with the first steps of insertion/addition reactions. The zero point vibrational energy (ZPE) corrected CCSD(T)/aug-cc-pVTZ level predicted potential energy diagrams through various interconnectivities between the abovementioned three insertion/addition reactions (*Channel-I* to *III*), where adduct intermediates or H_2SO_5 undergoes not only their unimolecular isomerizations but also the decompositions followed by isomerizations or vice-versa to produce various product molecules and radicals, as mentioned above, is shown in the Supplementary Fig. 1. In the potential energy diagrams, we also show additionally a possible route that may form SO_4 (Sulfur Tetroxide or Peroxide) + H_2O product molecules via the decomposition of SO_4¨H_2O complex in the singlet state, while the photolysis of SO_4 may result in the SO_2 + $O_2(^1\Delta_g)$. Similarly, the M06-2X/aug-cc-pVTZ level optimized geometries of various adducts, complexes and TSs involved in the potential energy diagrams (Supplementary Fig. 1) have been shown in the Supplementary Fig. 2. It should be noted here that we have considered the $O(^1D)$−insertion/addition reactions. Also, based on the mechanistic

aspects of every reaction step in the potential energy diagrams predicted at 0K, we find that the overall mechanism for these reactions are mainly the addition of O(^{1}D) and hydrogen atom transfer during the unimolecular isomerization and decomposition of the H_2SO_4−O(^{1}D) adducts or H_2SO_5 molecule to form final products. Given this, we also point out here that the barrierless (or near-barrierless) bimolecular collisions of a reaction pathway with large exothermicities at a particular temperature do not follow every reaction step sequentially and necessarily starting from the stable reaction intermediate involved in the first step. In particular, when the reaction intermediates and transition states, associated with the unimolecular isomerization or decomposition of that reaction intermediates of a reaction pathway, are close to in energy, the barrierless bimolecular collisions of that reaction pathway can result in the unstable geometrical configurations close to the transition states associated with the reaction intermediates; where near instantaneous hydrogen transfer and the addition of O(^{1}D) through bond breaking and making process can also trigger effectively the O(^{1}D)−insertion/addition reactions to form final product molecules. In addition, during two-body encounters between H_2SO_4 + O(^{1}D) reactants, the approach of O(^{1}D) towards H_2SO_4 may also cause the geometry reorganizations through the bond breaking and making process via the hydrogen atom transfer from the O−H functional group of H_2SO_4 to O(^{1}D) due to the hydrogen-bonding interaction within the pre-reactive H_2SO_4···O(^{1}D) complex without the direct addition/insertion reactions or via the additional and much more complicated reactions (which might have significant potential impacts) to produce abovementioned product molecules. This follows as the O(^{1}D) has reactivity not only towards its addition but also in the hydrogen abstraction. Nevertheless, we do not consider all these reaction mechanisms in the present work, as our first and main goal is to understand the potential atmospheric impact of the O(^{1}D)−insertion/addition reactions, especially, towards the loss of

H_2SO_4 molecule rather than the overall impact of all the potential energy diagrams involving all the reaction channels.

As mentioned above, we have referred the insertions or additions of $O(^1D)$ into the O−H, S=O and S−O bonds as the *Channel-I*, *Channel-II* and *Channel-III*. Given that the insertion/addition reactions has the potential to produce various product molecules including SO_2, we, however, note that energetically the most favourable pathways are those that lead to the formations of either H_2SO_5 (H_2SO_5-I or H_2SO_5-II) or SO_3 + H_2O_2 molecules. It is seen from the Supplementary Fig. 1 that while the *Channel-III* is capable of forming the H_2SO_5-II molecule directly, the *Channel-I* and *Channel-II* go through the adduct intermediates (Ad-I and Ad-II), and the energetically most favourable reaction pathways in the *Channel-I* and *Channel-II* are the paths involving TS-IA and TS-II (Supplementary Fig. 1). It is also worth noting here that the most stable product molecule in the insertion/addition reaction pathways via *Channel-I* to *III* is the H_2SO_5 (H_2SO_5-I or H_2SO_5-II) and second most stable product molecules are SO_3 and H_2O_2 resulting from the unimolecular decomposition of either Ad-I or H_2SO_5 (H_2SO_5-II). Also, the unimolecular barrier height for the conversion of the identical H_2SO_5 conformers (H_2SO_5-I), resulted via *Channel-I* and *Channel-II*, into the more stable H_2SO_5 conformer (H_2SO_5-II) is only ~3.1 kcal mol^{-1} (Supplementary Fig. 1). Therefore, the most stable product molecule in the *Channel-I* and *Channel-II* is also the H_2SO_5-II conformer of *Channel-III*. Moreover, it should be noted here that unlike H_2SO_5−II, the H_2SO_5−I formed via the *Channel-I* or *II* is not directly decomposed into the SO_3 + H_2O_2 molecules. This follows as the H_2SO_5−I requires the H_2SO_5−I → H_2SO_5−II conversion via internal rotation of the O−OH functional group before its decomposition starts from the H_2SO_5−II (Supplementary Fig. 2). However, as the unimolecular barrier height for the H_2SO_5−I → H_2SO_5−II interconversion is only ~3.1 kcal mol^{-1} and while the

energy of H_2SO_5–I with respect to the H_2SO_4 + O(^{1}D) reactants is −80 kcal mol^{-1}, the *Channel-I* or *II* via the formation of H_2SO_5–I can also equally contribute to the formation of SO_3 + H_2O_2 molecules (Supplementary Fig. 1).

It has been mentioned main article (Method section, Main Article) that the T_1 diagnostic cut off value for the closed- and open-shell systems are respectively ~0.020 and 0.045.[1-4] The T_1 diagnostic values for all the species involved in the potential energy diagram (Supplementary Fig. 1) at the CCSD(T)/aug-cc-pVTZ calculations have been given in Supplementary Table 3. It is seen from the Supplementary Table 3 that all the neutral closed-shell species, except TS-I, SO_2 and TS-VI are predominantly single reference in character, as their T_1 diagnostic values are found to be in the range from ~0.006 to ~0.020. Therefore, all the species, except TS-I, SO_2 and TS-VI, are treated well by the CCSD(T)/aug-cc-pVTZ level of calculations, and hence, the CCSD(T)/aug-cc-pVTZ level predicted energetics are reliable. Similarly, the relative energy of the open-shell HSO_4 radical (T_1 ~0.024) in the potential energy diagram is also expected to be reliable at the UCCSD(T)/aug-cc-pVTZ level of theory, as the T_1 diagnostic value is lower than the cut off value for an open-shell system (~0.045).[2-4] Among the TS-I, SO_2 and TS-VI, the T_1 diagnostic values of TS-I (T_1 ~0.022) and SO_2 (T_1 ~0.021) are very close to the cut off value for single reference system (0.020). Thus, although the TS-I and SO_2 might have slight multi-reference character, nevertheless, the CCSD(T)/aug-cc-pVTZ level predicted relative energetics of the TS-I and SO_2 with respect to other stationary points in the potential energy diagram should also be considered reliable enough (see below). It should be noted here that the reaction path involving TS-I in the *Channel-I* is not energetically the most favourable reaction path. The most favourable reaction path in the *Channel-I* is the path involving TS-IA of single reference in character (Supplementary Fig. 1 and Supplementary Table 3). In contrary, the TS-VI, especially

in comparison to all the species involved in the potential energy diagram, is expected to have significant multi-reference character, as its T_1 diagnostic value is ~0.030. We also find here that the TS-VI is less important as the TS-VI is not directly associated with the energetically most favourable reaction pathways, as discussed above. Nevertheless, we further perform the CASPT2/aug-cc-pVTZ//CASSCF/aug-cc-pVTZ calculations with (12,12) active space (12 electrons,12 orbitals), especially, to refine the relative energies not only for TS-VI but also for TS-I. In the CASPT2/aug-cc-pVTZ//CASSCF/aug-cc-pVTZ calculations, we perform the single point energy calculations at the CASPT2/aug-cc-pVTZ level using the CASSCF/aug-cc-pVTZ level optimized geometries with same active space, which we refer here as simply the CASPT2(12,12)/aug-cc-pVTZ level of calculations. It is to be noted here that we have also performed CASPT2//CASSCF calculation in conjunction with aug-cc-pVDZ basis set and with same active space. Nevertheless, to keep the discussion simple here, we highlight only the CASPT2(12,12)/aug-cc-pVTZ level predicted results. The zero point vibrational energy (ZPE) corrections in the CASPT2(12,12)/aug-cc-pVTZ level have been done from the ZPE corrections predicted at both the CASSCF(12,12)/aug-cc-pVTZ and M06-2X/aug-cc-pVTZ levels of theories. It is seen from our calculations that the ZPE corrected energies at the CASPT2(12,12)/aug-cc-pVTZ level are consistent with respect to the ZPE corrections at both the CASSCF(12,12)/aug-cc-pVTZ and M06-2X/aug-cc-pVTZ levels of theories. Therefore, we highlight here only the ZPE corrected energies at the CASPT2(12,12)/aug-cc-pVTZ level according to the CASSCF(12,12)/aug-cc-pVTZ level predicted ZPE correction. It should be noted here that the TS-I and TS-VI are directly associated with the Ad-I → H_2SO_5-I and Ad-IIA → H_2SO_5-II unimolecular reaction steps, respectively (Supplementary Fig. 1 and 2). Therefore, we perform the CASPT2(12,12)/aug-cc-pVTZ level calculations for the Ad-I, TS-I, H_2SO_5-I,

Ad-IIA, TS-VI and H_2SO_5-II, although the Ad-I, H_2SO_5-I, Ad-IIA and H_2SO_5-II are predominantly single reference in character. In addition, we also calculate the energetics of the $H_2SO_4 + O(^1D)$ reactants in the *Channel-I* at the CASPT2(12,12)/aug-cc-pVTZ level of theory to compare the energetics of the reaction path involving TS-I at both the CCSD(T)/aug-cc-pVTZ and CASPT2(12,12)/aug-cc-pVTZ calculations. It should also be noted here that the reaction coordinate with respect to the bonds breaking and making process associated with the Ad-I → H_2SO_5-I unimolecular reaction step via TS-I is different from that involved in the Ad-IIA → H_2SO_5-II unimolecular reaction step via TS-VI. Hence, the choice of active space for Ad-I → H_2SO_5-I conversion via TS-I was different from that in the case of Ad-IIA → H_2SO_5-II conversion via TS-VI. In other words, for the calculation of energy of TS-I with respect to Ad-I, we construct a common active space that describes both the TS-I and Ad-I, and this active space is different from that has been constructed for the calculation of energy of TS-VI with respect to Ad-IIA. The approximate description of orbitals involved in the (12,12) active space for different reaction steps have been given in Supplementary Table 4. Similarly, the CASPT2(12,12)/aug-cc-pVTZ level predicted energetics of the reaction steps, as mentioned above, has been shown in Supplementary Fig. 3. In our CASPT2(12,12)/aug-cc-pVTZ calculations, we did not find any transition state corresponding to the TS-VI associated with the Ad-IIA → H_2SO_5-II unimolecular step, but we locate a different transition state, which is involved in the Ad-IIA → $HSO_4^{\cdots}OH$ unimolecular step. This has been verified through IRC calculations at the CASSCF(12,12)/aug-cc-pVDZ level of theory. We label this different transition state as the TS-VIA (Supplementary Fig. 3) and the CASPT2(12,12)/aug-cc-pVTZ level predicted unimolecular barrier height including ZPE corrections for the Ad-IIA → $HSO_4^{\cdots}OH$ conversion via TS-VIA is ~17.94 kcal mol^{-1}. Importantly, when we consider this TS-VIA, located at the CASPT2(12,12)/aug-cc-pVTZ

level of calculation, as the initial guess and re-optimize the transition state at M06-2X/aug-cc-pVDZ and M06-2X/aug-cc-pVTZ levels of theory, the calculations end up with the location of same TS-VI, as mentioned above. Given this, we also note here that the Ad-IIA $\rightarrow$ HSO_4···OH unimolecular step via TS-VIA is energetically an unfavourable path in comparison to the path associated with TS-II in the *Channel-II*. This is because of relatively large unimolecular barrier height associated with the TS-VIA in comparison to that in TS-II. It should be noted here that the energetically the most favourable reaction pathway in *Channel-II* is the path involving TS-II, as mentioned above.

In the case of *Channel-I*, it is seen from our CASPT2(12,12)/aug-cc-pVTZ calculations including ZPE corrections that the unimolecular barrier height for the Ad-I $\rightarrow$ H_2SO_5-I conversion via TS-I or the energy of TS-I with respect to Ad-I is ~2.1 kcal mol^{-1}. The corresponding value at the CCSD(T)/aug-cc-pVTZ level of calculation is ~3.2 kcal mol^{-1}. Similarly, the energy of the Ad-I and H_2SO_5-I with respect to the total energy of the H_2SO_4 + $O(^1D)$ reactants in the *Channel-I* at the CCSD(T)/aug-cc-pVTZ level of calculations are respectively ~25.5 and ~80 kcal mol^{-1}. The corresponding values at the CASPT2(12,12)/aug-cc-pVTZ level of theory are respectively ~23.2 and ~76.2 kcal mol^{-1}. Therefore, the CCSD(T)/aug-cc-pVTZ and CASPT2(12,12)/aug-cc-pVTZ levels predicted results for the *Channel-I* involving TS-I are consistent to each other. This was expected, as the T_1 diagnostic value of TS-I is ~0.022, and this value is very close to the cut off value for single reference system (0.020).

In addition, we also note that while the insertion/addition of $O(^1D)$ into the S−O bond of H_2SO_4 (*Channel-III*) changes the geometrical identity of the H_2SO_4 through the formation of H_2SO_5 molecule in a single step, the first step of the insertions/additions of $O(^1D)$ into the O−H and S=O bonds of H_2SO_4 (*Channel-I* and *II*) forms the adduct intermediates (H_2SO_4−$O(^1D)$ ≡

Ad) keeping the geometrical identity of the H_2SO_4 molecule somewhat intact. Therefore, we also predict the **approximate** potential energy curves representing the barrierless H_2SO_4 + $O(^1D)$ addition reactions for the formations of Ad-I and Ad-II at the CASPT2(12,12)/aug-cc-pVDZ//CASSCF(12,12)/aug-cc-pVDZ level of theory by scanning the O···O distances along the O−O bonds of the Ad-I and Ad-II [Insertions/additions of $O(^1D)$ into the O−H or S=O bond via *Channel-I* and *Channel-II*] from their equilibrium bond distances to ~5Å at step size 0.1Å and keeping the optimized geometrical parameters of the H_2SO_4 subunit in the Ad-I and Ad-II fixed. The calculated approximate potential energy curves representing the barrierless addition reactions at the CASPT2(12,12)/aug-cc-pVDZ//CASSCF(12,12)/aug-cc-pVDZ level of theory have been shown in the Supplementary Fig. 4. It is to be noted here that a similar scan for the *Channel-III*, the scan of **O** atom from the S–**O**–OH functional group of H_2SO_5 molecule, would not provide the approximate potential energy curve representing the barrierless H_2SO_4 + $O(^1D)$ insertion reaction for the formation of H_2SO_5 molecule directly. This follows as the scan of **O** atom from the S–**O**–OH functional group causes a well-separated distance between the HSO_3• and OH• fragments present in the H_2SO_5 molecule, and hence, the scan would result in the HSO_3• + $O(^1D)$ + OH• reactants instead of starting H_2SO_4 + $O(^1D)$ reactants. As mentioned above that the insertion/addition of $O(^1D)$ into the S−O bond of H_2SO_4 (*Channel-III*) changes the geometrical identity of the H_2SO_4 through the formation of H_2SO_5 molecule in a single step. Given this, we also note while the scan of **O** atom from the S–**O**–OH functional group causes a well-separated distance between the HSO_3• and OH• fragments present in the H_2SO_5 molecule formed in the *Channel-III*, the formation of S−$O(^1D)$ (or S−O) bond in the Ad-II via the *Channel-II* occurs by keeping the geometrical identity of the H_2SO_4 molecule somewhat intact. Therefore, we also calculate the approximate potential energy curve representing the barrierless

interaction between H_2SO_4 + O(^{1}D) reactants along the S−O coordinate of Ad-II. Like before, here we obtain the potential energy curve by scanning the S···O distance along the S−O bond of the Ad-II from its equilibrium bond distance to ~5Å at step size 0.1Å and keeping the optimized geometrical parameters of the H_2SO_4 subunit in the Ad-II fixed. The calculated potential energy curve along the S−O bond of the Ad-II has also been shown in the Supplementary Fig. 4. Similarly, the approximate description of active spaces used in the scan calculations has also been given in the Supplementary Table 4. Overall, we find here that the CASPT2//CASSCF level of calculations supports further the prediction of the CCSD(T) level. As a result, to keep our discussion simple in the main article, we only highlight the results predicted at the CCSD(T)/aug-cc-pVTZ level of theory unless otherwise stated the specific levels of calculations.

Moreover, we also explore the stability of ground state adducts (Ad-I and Ad-II) and H_2SO_5 in the first two low-lying excited states for the H_2SO_4 + O(^{1}D) reaction through various calculations at UCIS, CASSCF and TDDFT levels of theories. For the first excited state, we employ all three levels of theories and we perform CASSCF calculation with (10,10) and (10,8) active space. While for the second excited states, we use UCIS and TDDFT levels of theories. In the case of TDDFT calculations, we use UM06-2X functional. We mainly focus upon adducts and H_2SO_5 because the formation of these strongly bound adducts or H_2SO_5 molecule in excited states with typical fast bimolecular rate constants (10^{-10} cm^3 molecule^{-1} s^{-1}), which we have predicted for the ground state (see below), can only make an important contribution comparable to that of ground state. In other words, in the case of all the excited state reaction mechanisms with just one to two orders of magnitude smaller rate constants (10^{-11} or 10^{-12} cm^3 molecule^{-1} s^{-1}), the reaction contribution between ground state and excited state becomes either 10:1 (100%:10%) or 100:1 (100% :1%). As a result, it is important to explore the stability of strongly

bound adducts (Ad-I and Ad-II) and H_2SO_5 in the excited states. It is seen from our calculations that the O−O(^{1}D) bond in adducts and −O−O− bond in H_2SO_5 are repulsive for their formations in both the first and second excited state, and the overall findings is very much similar to the potential energy diagrams associated with the photodissociation of peroxides or peroxyacid molecules, which are stable in ground state and unstable in excited states.[5-14] Hence, we conclude that the H_2SO_4 + O(^{1}D) insertion/addition reactions predominantly occur in the ground singlet potential energy surface similar to the H_2 + O(^{1}D), HCl + O(^{1}D) or CH_4 + O(^{1}D) reaction systems.[15-19]

Next, we focus mainly on kinetics of energetically the most favourable reaction pathways according to potential energy diagrams predicted at 0K. In addition, we also consider here the formation of H_2SO_4-I from the Ad-I and the SO_3 + H_2O_2 molecules from the H_2SO_4-II molecule (Figure 1, Main Article). This follows because the Ad-I formed in the *Channel-I* is expected to isomerize further to form the H_2SO_4-I. Similarly, H_2SO_5-II formed in the *Channel-III* is expected to decompose further to form the SO_3 + H_2O_2 molecules. Therefore, the reactions that form the adduct intermediates or H_2SO_5 in the first steps and which then further in the second steps produce respectively the H_2SO_5 or SO_3 + H_2O_2 molecules can be represented in general form as follows:

$$H_2SO_4 + O(^1D) \underset{k_{-1}}{\overset{k_1}{\rightleftharpoons}} INT \xrightarrow{k_2} P \qquad (1)$$

For *Channel−I*, the INT and P in the above equation 1 are respectively the H_2SO_4−O(^{1}D) adduct intermediate (Ad-I) and either SO_3 + H_2O_2 molecules or H_2SO_5 (H_2SO_5-I). It should be noted here that the Ad-I in *Channel−I* through TS-IA and TS-I forms respectively the SO_3 + H_2O_2

molecules and H_2SO_5 (H_2SO_5-I). Similarly, for *Channel−II*, the INT and P in the above equation 1 are respectively the Ad-II and H_2SO_5 (H_2SO_5-I). In the case of *Channel−III,* the INT is simply the H_2SO_5-II conformer, as there is no reaction intermediate or adduct involved in the first step of reaction, and P is the SO_3 + H_2O_2 molecules. The k_1 and k_{-1} are respectively the association rate constant (cm^3 $molecule^{-1}sec^{-1}$) for the formation of INT in the addition/insertion reactions between the H_2SO_4 + $O(^1D)$ reactants and decomposition rate constant (sec^{-1}) of the INT to from back into the isolated H_2SO_4 + $O(^1D)$ reactants. For the *Channel−I* and *II*, the k_2 is the unimolecular rate constant (sec^{-1}) for the isomerization of INT [≡ Ad-I or Ad-II] via the transition states (TSs) to form either the SO_3 + H_2O_2 molecules (*Channel-I*) or the H_2SO_5-I conformer (*Channel-I* and *Channel-II*) as the product molecules. Similarly, for the *Channel−III*, the k_2 is the unimolecular rate constant (sec^{-1}) for the decomposition of INT (≡ H_2SO_5-II conformer) via the transition state (TS) to form the SO_3 + H_2O_2 as the second most stable product molecules. Applying the steady state approximation[20] on the concentration of INT [≡ H_2SO_4−$O(^1D)$ or H_2SO_5-II)] formed in the potential energy diagrams, the overall rate constant (k) of the abovementioned insertion/addition reactions can be expressed as:

$$k = \frac{k_1}{k_{-1} + k_2}\ k_2 \qquad (2)$$

In the equation 2, the overall rate constant (k) becomes (k_1k_2/k_{-1}), when $k_{-1} >> k_2$. Moreover, the ratio of the association and decomposition rate constants of INT (k_1/k_{-1}) can be expressed as the K_{eq}, where K_{eq} is the equilibrium constant for the formation of INT from the isolated H_2SO_4 + $O(^1D)$ reactants. Therefore, when $k_{-1} >> k_2$, the overall rate constant (k) becomes $K_{eq}k_2$, On the other hand, when $k_{-1} << k_2$, the overall rate constant simply becomes the association rate constant (k_1) for the formation of the INT from the isolated H_2SO_4 + $O(^1D)$ reactants. Therefore, it is

important to estimate the k_1 and K_{eq} for the first steps of reactions, and the k_2 for the second steps of reactions to understand the overall kinetics of the reactions (see Supplementary Note-2) that go through the reaction intermediates or stable product molecules, as mentioned above.

Supplementary Note-2. The rate constants at standard pressure of 1bar for the three reactions pathways (*Channel-I*, *II* and *III*), as mentioned here (or Main Article), have been calculated by the variational transition state theory (VTST) implemented in the Polyrate−2010 and Gaussrate−2009 program packages.[21-22] While the reaction path−VTST (RP-VTST) have been used to calculate the rate constants for the reaction steps associated with the well defined transition states (TSs) or potential energy barriers, the association rate constants for the barrierless insertion or direct addition reactions [H_2SO_4 + $O(^1D)$] have been calculated using the variable reaction coordinate−VTST (VRC-VTST).[23-31] The M06-2X functional in conjunction with the 6-31G* basis set has been used to predict the association rate constants of the insertion/addition reactions in the formalism of energy (E) and angular momentum (J) resolved micro-canonical variational transition state theory (E,J-μVT).[21-22] Moreover, the fivefold degeneracy of $O(^1D)$ has been taken into account in predicting the association rate constants for the barrierless insertion/addition reactions. In other words, we have used the electronic degeneracy of $O(^1D)$ = 5 in our VRC-VTST calculations. To compute the rate constants for the reactions with potential energy barriers, the Minimum Energy Path (S) has been constructed in the range of 1.0 Å < S < 1.0 Å using Page–McIver integrator[32] with a step size of 0.1 Å. In the calculations of association rate constants between the H_2SO_4 and $O(^1D)$ reactants using VRC-VTST, we optimize the minimum energy reaction coordinate (S) between the pivot points located near the H_2SO_4 and $O(^1D)$ reactants in the range from 2.0 Å to 6 Å with step size of 0.2 Å, and the minimized association rate constants in the 100-400K temperature range have been

obtained by varying the locations of pivot points[24-25,30-31] placed on the each of the two reactants. Moreover, the multi-faceted dividing surface have been generated by choosing two pivot points near the O atom of O−H bond (for *Channel-I*), O atom of S=O bond (for *Channel-II*) and S atom (for *Channel-III*) of the H_2SO_4 and one pivot point on the O(^{1}D) reactant. This is because the multi-faceted dividing surface predicted association rate constants are more accurate than that predicted from the single-faced dividing surface.[24-25,33] Also, the multi-faceted dividing surface for a particular interacting atom of a polyatomic molecule and O(^{1}D) in a reaction pathway among the multiple reaction pathways is expected to cover all the possible interactions in the coordinate space[21-22] associated with that particular interacting atom of that polyatomic molecule and O(^{1}D). To understand the pivot point configurations in generating the multi-faceted dividing surface for a particular reaction pathway, we highlight here the configuration of pivot points for *Channel-I* as an example. In the case of insertion of O(^{1}D) into the O−H bond of the H_2SO_4 molecule via *Channel-I*, we have chosen two pivot points on both the directions from the oxygen atom along an axis that goes through oxygen atom and one pivot point on the O(^{1}D) (Supplementary Fig. 5). Overall, to get the minimum values rate constants for the *Channel-I* to *III*, the maximum seven sets of pivot points with respect to different locations of two pivot points near the O or S atoms are chosen and the distances of two pivot points near the O or S atoms were at 0.25, 0.5, 1.0, 1.25, 1.50, 1.75 and 2.0 Å. In the case of *Channel-I*, it is seen from our calculations that when we place two pivot points near the oxygen atom of the O−H bond at 1.50 Å, we obtain the minimum values of rate constants in the temperature range from 100 to 360K (see Supplementary Table 5) and likewise, when we set the pivot points at 1.25 Å, we obtain the minimum values of rate constants in the temperature range from 340K to 400K (see Supplementary Table 5). In contrary, when we chose two pivot points at a distance smaller or

greater than 1.50 or 1.25 Å away from the oxygen atom of the O−H bond, we obtain slightly higher values of rate constants (Supplementary Table 5). It is also worth noting here that we have chosen similar but separate sets of pivot points on the H_2SO_4 molecule for the *Channel-II* and *III*. It is seen from our calculations that in the case of *Channel-II*, when we place two pivot points respectively at 1.50 and 1.75 Å near the oxygen atom of the S=O bond, similar to the configuration as shown Supplementary Fig. 5, we obtain the minimum values of rate constants in the temperature range from 100K to 400K (Supplementary Table 6). Similarly, the optimized distances of two pivot points in the case of *Channel-III* are 0.50 and 1.00 Å (Supplementary Table 7). The E,J-μVT predicted minimized association rate constants for the *Channel-I* to *III* with respect to the optimized pivot points are given in the Supplementary Table 8 in the temperature range from 100 to 400K.

Moreover, to estimate the overall rate constants (k) of the H_2SO_4 + $O(^1D)$ reactions for the formation of SO_3 + H_2O_2 molecules via Ad-1 (*Channel-I*), H_2SO_5 via Ad-I and Ad-II (*Channel-I* and *II*), and SO_3 + H_2O_2 from the H_2SO_5-II (*Channel-III*), the unimolecular rate constants (k_2) for the decomposition of the Ad-I (Ad-I → SO_3 + H_2O_2), isomerizations of the Ad-I and Ad-II (Ad-I or Ad-II → H_2SO_5-I), and decomposition of the H_2SO_5-II (H_2SO_5-II → SO_3 + H_2O_2) through RP-VTST have been calculated within canonical variational transition state theory including small curvature tunnelling correction (CVT/SCT).[21-22] To get the refined values of the CVT/SCT predicted rate constants for the unimolecular reaction steps, we use CCSD(T)/aug-cc-pVTZ level predicted reaction energetics. The temperature dependent equilibrium constants (K_{eq}) according to the energies predicted at the CCSD(T)/aug-cc-pVTZ level of theory and the CVT/SCT predicted rate constants for the unimolecular reaction steps have been given in the Supplementary Table 8 to 9.

It is seen from the equation 2 (Supplementary Note-1) using all the data in Supplementary Table 8 and 9 that the overall rate constants (k) in the temperature from 100 to 400K for the three channels are the association rate constants in the first step (k_1), as $k_{-1} << k_2$. It is to be noted here that the k_2 for the unimolecular Ad-I → H_2SO_5-I isomerization step via TS-I in *Channel-I* at the CASPT2(12,12)/aug-cc-pVTZ level of calculation is slightly faster than that predicted at CCSD(T)/aug-cc-pVTZ level of theory (Supplementary Table 9). This follows as the unimolecular barrier height at the CASPT2(12,12)/aug-cc-pVTZ level of calculation is slightly lower than that predicted at the CCSD(T)/aug-cc-pVTZ level of theory, as mentioned earlier. However, the overall conclusion is that the association rate constants in the first step (k_1) are the overall rate constants (k) for the three channels, as mentioned above. Given that the insertion/addition are fast reactions at standard pressure of 1 bar, we next focus upon the both the temperature and pressure dependency of the overall rate constants (k) in various atmospheric temperatures and pressures (see Supplementary Note-3).

Supplementary Note-3. From the kinetics analysis presented above, it is seen that the H_2SO_4 + $O(^1D)$ association steps, the first steps in the *Channel-I* to *III*, control the overall reactions at standard pressure of 1 bar. It is also seen from the literature that the overall rate constants for barrierless association or addition reactions with large exothermicities are pressure independent, especially, at low atmospheric pressures.[34-40] Nevertheless, to verify this in the present case of insertion/addition reactions, we first consider that the *Channel-I* to *III* terminates in the first step, especially, to understand the extent of exothermicity at which the rate constants are pressure independent at atmospheric pressures. In other words, we assume that the H_2SO_4−$O(^1D)$ adducts (Ad-I and Ad-II) in the *Channel-I* and *II*, and the H_2SO_5-II in the *Channel-III* are the sinks of the reactions, and examine the extent of pressure dependency of rate constants with respect to

various exothermicities of the reaction steps. Here, we approximately describe the potential energy difference between the reactants and products as the exothermicity of the reaction. To examine the extent of pressure dependency of rate constants with respect to various exothermicities of the reaction steps, we explore the pressure variations of the temperature dependent VRC-VTST predicted rate constants using the Master Equation Solver for Multi-Energy Well Reactions (MESMER)[41] program, especially, at low atmospheric pressures. In MESMER run, we chose the ILT (Inverse Laplace Transformation) method for the barrierless reaction steps and the VRC-VTST predicted rate constants as the initial guess for the barrierless reaction steps. Note here, for a particular altitude of the Earth's atmosphere, we chose the VRC-VTST predicted rate constant corresponding to the atmospheric temperature of that particular altitude as the initial guess. The MESMER runs with a deficient reactant and excess reactant, and in the present case, we select the $O(^1D)$ as deficient reactant (1 molecule cm^{-3}) and H_2SO_4 as the excess reactant in presence of N_2 as bath gas maintaining the actual atmospheric pressures at different altitudes. Here, the concentration of H_2SO_4 at a particular altitude, as excess reactant, is fixed according to its atmospheric concentration at that particular altitude. For example, at 40, 50 and 60 km altitudes, the concentrations of H_2SO_4, as excess reactant, are respectively ~1.6×10^7, 1.6×10^6 and 7.2×10^5 molecules cm^{-3}. It has been mentioned above that the H_2SO_4–$O(^1D)$ adducts (Ad-I and Ad-II) in the *Channel-I* and *II*, and the H_2SO_5-II in the *Channel-III* are considered as the sinks of the reactions with the assumption that the reactions terminate in the first steps. Given this, we consider the pseudo first order rate of $O(^1D)$ loss in the reactions at different altitudes of the Earth's atmosphere. Note here that the pseudo first order rate of $O(^1D)$ loss means the loss of single $O(^1D)$ atom in presence of excess or fixed atmospheric concentrations of H_2SO_4 per cm^3 and per unit time (sec^{-1}). Also, in the H_2SO_4 + $O(^1D)$

association steps, the overall reaction rate for each reaction step is equal to the loss of either $O(^1D)$ or H_2SO_4 per unit time. At the same time, the overall rate of the $H_2SO_4 + O(^1D)$ reaction can be expressed as: $k * [H_2SO_4] * [O(^1D)]$, where k is overall rate constant of the reaction. Therefore, the pseudo first order rate of $O(^1D)$ loss can be written as: $k' * [O(^1D)]$, where $k' = k * [H_2SO_4]$, and when concentration of $O(^1D)$ is 1 molecule cm^{-3}; $k' * [O(^1D)] = k'$. Therefore, the overall bimolecular rate constants (k) can be extracted from the pseudo first order rate of $O(^1D)$ loss in presence of fixed atmospheric concentrations of H_2SO_4 at different altitudes. In Supplementary Table 10 to 12, we present the atmospheric pressures from 0 to 110 km altitudes of Earth's atmosphere, VRC-VTST predicted rate constants relevant to 0 to 110 km altitudes that have been used in the MESMER as initial guesses, pseudo first order rate of $O(^1D)$ loss, atmospheric concentrations of H_2SO_4 and the extracted overall rate constants (k) from the MESMER calculations for the first reaction steps in the *Channel-I* to *III*. It should be noted here that above 60 km altitude of Earth's atmosphere, the concentrations of H_2SO_4 are unknown. Nevertheless, we consider here the atmospheric mixing ratios of H_2SO_4 by volume above 60 km altitude are constant, especially, for an understanding the extent of pressure independency of the VRC-VTST predicted rate constants with respect to different exothermicities of the reaction steps. For *Channel-I*, it is seen from the Supplementary Table 10 that the VRC-VTST predicted rate constants (k_1) is very much pressure independent from 0 to 25 km altitude of Earth's atmosphere (corresponds to 1 to 0.025 atm pressure), as both the VRC-VTST predicted rate constants (k_1) and overall rate constants (k), extracted from the MESMER program, are comparable to each other. After 25 km altitude, the k_1 is pressure sensitive. Similarly, in the case of *Channel-II* (Supplementary Table 11) the k_1 is very much pressure independent from 0 to 65 km altitude of Earth's atmosphere (corresponds to 1 to 1.09×10^{-4} atm pressure), and for

Channel-III, the k_1 is pressure independent from 0 to 110 km altitude of Earth's atmosphere (corresponds to the 1 to 7.01 x 10^{-8} atm pressure, Supplementary Table 12). This is expected as the relative energies, which we called here as the exothermicities, of the Ad-I, Ad-II and H_2SO_5-II in the *Channel-I* to *III* are respectively ~25.5, ~46.6 and ~82.6 kcal mol^{-1}. Therefore, we not only come to the same conclusion as mentioned above through literature that the rate constant for the fast barrierless association reaction are pressure independent in low atmospheric pressures; but also in the fact that the extent of this pressure independency of rate constants depends upon the extent of exothermicities associated with the reaction steps. Given this, we also know that the Ad-I or Ad-II cannot be treated as the sinks in the *Channel-I* and *II*, as the unimolecular barrier heights for the Ad-I → SO_3 + H_2O_2 and Ad-II → H_2SO_5-I are respectively and only ~1.0 and ~4 kcal mol^{-1}, and while the relative energies of the TSs associated with these two unimolecular reaction steps with respect to the total energy of the H_2SO_4 + $O(^1D)$ reactants are respectively ~ −24.5 and ~ −42.6 kcal mol^{-1}. Therefore, we next calculate the pseudo first order loss of $O(^1D)$ by considering the SO_3 + H_2O_2 and H_2SO_5-I as the sinks in the *Channel-I* and *II*. In contrast to the *Channel-I* and *II*, we find that the H_2SO_5-II in the *Channel-III* can be consider as the sink, especially, at extremely cold conditions with high pressure of buffer gases like supersonic jet or matrix isolation environments. However, in the Earth's upper atmosphere, where collision rates are less, the SO_3 + H_2O_2, similar to H_2SO_5-II, may also expected to be the sinks, as the exothermicity associated with the first step in the *Channel-III* is the highest and very large in comparison to that in case of *Channel-I* and *Channel-II*. Therefore, we also calculate the pseudo first order loss of $O(^1D)$ by considering the SO_3 + H_2O_2 as the sinks in the *Channel-III*. Like before, here also in the MESMER run, we chose the ILT (Inverse Laplace Transformation) method for the barrierless reaction steps and use the VRC-VTST predicted rate constants as the

initial guess for the barrierless first reaction steps. Also, we consider the Ad-I and SO_3¨H_2O_2 product complex in the *Channel-I*, and Ad-II in *Channel-II* are the 'Modelled' and use the RRKM theory for the prediction of rate constants associated with the unimolecular Ad-I → SO_3 + H_2O_2 and Ad-II → H_2SO_5-I reaction steps. Similarly, for *Channel-III*, the H_2SO_5-II and SO_3¨H_2O_2 product complex are considered as the 'Modelled' and use the RRKM theory for the prediction of rate constants associated with the unimolecular H_2SO_5-II → SO_3 + H_2O_2 reaction step. It should be noted here that the Lennard-Jones (L-J) potential has been used to model the interaction between the 'Modelled' [H_2SO_4–O(^{1}D) adducts (Ad-I and Ad-II), H_2SO_5-II or SO_3¨H_2O_2 product complex] and bath gas. The L-J parameters σ and ε/k_B has been calculated using the following equations.[42]

$$\sigma = 2.44(T_C/P_C)^{1/3} \qquad (3)$$

$$\varepsilon/k_B = 0.77T_C \qquad (4)$$

In the equation 3 and 4, the T_C and P_C are respectively the critical temperature and pressure. The k_B is the Boltzmann constant. Like before, we provide three tables (Supplementary Table 13 to 15) that represent the comparison of VRC-VTST predicted rate constants and overall rate constants of the reactions extracted from the pseudo first order rate of O(^{1}D) loss. From the comparison between k_1 and k in the Supplementary Table 13 to 15, it is seen that the k_1 is pressure independent from 0 to 110 km of altitudes (corresponding pressures 1 to 7.01 x 10^{-8} atm) for all three channels. This is expected as the effective exothermicities, energy difference between H_2SO_4 + O(^{1}D) reactants and sinks, for all the three reactions via *Channel-I* to *III* are more-or-less equal and very large. Thus, we confirm that the VRC-VTST predicted rate constants are pressure independent at atmospheric pressures, and we use the VRC-VTST

predicted minimum values of k_1 (= k) to explore the potential impact of the H_2SO_4 + $O(^1D)$ reactions from 30 to 110 km altitudes of the Earth's atmosphere (see Supplementary Note-4).

Supplementary Note-4. The potential atmospheric impact of the insertion/addition reactions has been explored with respect to simple relative rate analysis. We mainly focus here upon the overall rate constants (k=k_1) of *Channel-I* to *III* to interpret the loss or decomposition of H_2SO_4 molecule in upper stratosphere and lower mesosphere (35 to 65 km) of the Earth's atmosphere, especially, where the atmospheric concentrations of H_2SO_4 are one to two orders of magnitude higher than those present in lower stratosphere of the Earth's atmosphere.[43-44] Importantly, it should also be noted here that the concentrations of ozone, which forms the $O(^1D)$ in presence of sunlight, are found to be large (4×10^{10} to 5×10^{12} molecule cm^{-3}) throughout the stratosphere (~10 to 50 km) of the Earth's atmosphere,[45-46] and the present insertions/additions mechanism is expected be the new physical insight in understanding further the claim or sensitivity of the ozone depletion in the geoengineering scheme of global climate using man-made injected stratospheric sulphate aerosols (see Main Article).

In the case of solar-pumping photolysis of H_2SO_4, the rate (ν) for the loss or decomposition of H_2SO_4 molecule can be written as: $\nu_{Photolysis} = J^*[H_2SO_4]$, where J is the photolysis rate coefficients via either UV or visible or Lyman−α radiation photolysis or photo-dissociation. Similarly, the rate for the loss or decomposition of H_2SO_4 molecule via the insertion/addition reactions with reaction degeneracy (σ) can be written as: $\nu_{Insertion} = \sigma[k_{(Channel\text{-}I)} + k_{(Channel\text{-}II)} + k_{(Channel\text{-}III)}]^*[H_2SO_4]^*[O(^1D)] = \sigma k_{(Total)}^*[H_2SO_4]^* [O(^1D)]$, where $k_{(Total)} = [k_{(Channel\text{-}I)} + k_{(Channel\text{-}II)} + k_{(Channel\text{-}III)}] = [k_{1(Channel\text{-}I)} + k_{1(Channel\text{-}II)} + k_{1(Channel\text{-}III)}]$. Moreover, while the fivefold degeneracy of $O(^1D)$ might play an important role in bimolecular reaction (see Main

Article), we only considered here the statistically distributed minimum 20% steady-state atmospheric concentration of $O(^1D)$ for the H_2SO_4 + $O(^1D)$ insertion/addition reactions. Therefore, the $\nu_{Insertion}/\nu_{Photolysis} = \sigma[k_{(Total)}/J]*[O(^1D)/5]$ is the simple equation by which we evaluate the potential atmospheric impact of the insertion/addition reactions over the various solar induced photolysis or photo-dissociation of H_2SO_4.

In Supplementary Table 16, we present the values of $\nu_{Insertion}/\nu_{Photolysis}$ from 30 to 110 km altitudes of the Earth's atmosphere, although our main focus is in the upper stratosphere and lower mesosphere of the Earth's atmosphere, as mentioned above. In our calculations, we consider the corrected *J* values for visible solar pumping photolysis of H_2SO_4 that has been derived by Miller et al. from the different photolysis quantum yields (in%) at different altitudes[47] and the *J* values derived from the experimentally measured overtone cross-sections (30 to 50 km altitude) with the assumption of quantum yield = 1 at all wavelengths.[48] We also consider the reported *J* values for the UV photolysis[49] using empirically derived UV absorption cross sections of 10^{-21} cm^2 $molecule^{-1}$ (upper limit)[50] between 179 and 226 nm. Importantly, from the work of Lane and Kjaergaard, we note that the dominant photo-dissociation mechanism of H_2SO_4 above 70 km is the absorption of Lyman−α radiation by high energy Rydberg excited states and that the photodissociation of H_2SO_4 via absorption in the UV region is unlikely to contribute significantly in the atmosphere.[51] It is seen that the *J* values using empirically derived UV absorption cross sections[49] in comparison to the theoretically predicted[51] *J* values in 60 to 80 km altitude range are two to three orders of magnitude higher (Supplementary Table 16). Finally, we also incorporate the *J* values predicted by Lane and Kjaergaard[51] for the absorption of Lyman−α radiation, while this mechanism is dominant above 70 km.

It should be noted here that the list of corrected *J* values for visible photolysis are not available in the work reported by Miller et al.;[47] but the corrected *J* values have been extracted from their work through graphical estimate using the *J* values for the UV photolysis as the reference.[49] Similarly, we also extract the *J* values for both UV and Lyman−α radiation from the work of Lane and Kjaergaard[51] as the list of values are not available. To the best of our knowledge, it should also be noted here that the *J* values for Lyman−α photo-dissociation, as mentioned above, are not known above 100 km altitude of the Earth's atmosphere. Nevertheless, only to get an idea about the $\nu_{Insertion}/\nu_{Photolysis}$ ratios above 100 km altitude in the case of Lyman−α photo-dissociation, we assume that the *J* values are constant from 100 to 110 km altitude of the Earth's atmosphere. Overall, it is seen from the Supplementary Table 16 that the $\nu_{Insertion}$ with 20% steady-state $O(^1D)$ concentration [≡ $O(^1D)/5$] is competitive with visible photolysis in the upper stratosphere and lower mesosphere of Earth's atmosphere, especially, when we consider the corrected *J* values. Similarly, above 70 km, only the photo-dissociation of H_2SO_4 via absorption of Lyman−α radiation is predominant mechanism even when we consider the 100% steady state concentration of $O(^1D)$.

Supplementary Note-5. Hence, it is seen from the above results and discussion that the $\nu_{Insertion}$ is competitive over the $\nu_{Photolysis}$ in the upper stratosphere, especially, when we consider 20% steady state concentration of $O(^1D)$, and when the $H_2SO_4 + O(^1D)$ encounters are mostly involved in the insertion/addition reactions. In reality, all $H_2SO_4 + O(^1D)$ encounters would not be involved in the insertion/addition reactions to form various product molecules; rather some fraction of the $H_2SO_4 + O(^1D)$ encounters may also result in $O(^1D) \rightarrow O(^3P)$ collisional quenching and $O(^1D) \rightarrow O(^1D)$ nonreactive scattering. Given this, we finally perform the direct dynamics trajectory surface hopping (TSH) calculations[52] in the ground state to estimate the

contribution of quenching and nonreactive scattering, if any, in the present study. It is seen from our existing results of trajectory surface hopping calculations with 390 trajectories that the 85% encounters are involved in reaction. Only ~1% $O(^1D) \rightarrow O(^3P)$ quenching and ~14% H_2SO_4 + $O(^1D)$ encounters are involved in nonreactive scattering. Therefore, the results of TSH calculations also support equally that the $H_2SO_4 + O(^1D)$ insertion/addition reactions competitive with the visible solar radiation pumping photolysis of H_2SO_4 vapor ($H_2SO_4 + h\nu \rightarrow SO_3 + H_2O$), especially, towards the loss of H_2SO_4 molecule in the upper stratosphere of the Earth's atmosphere. We understand that much more trajectories are required to get more accurate statistics, particularly, for the branching ratios of different products; however, we defer these works for future. It should be noted here that in our TSH calculations, the approximate relative translational energy (E_T) of colliding $O(^1D)$ with respect to H_2SO_4 is taken to be kT (= 0.02568 eV), corresponding to room temperature.

Regarding the details of TSH calculations, our molecular dynamics code is interfaced with Gaussian 09 computer program[53] in order to calculate the potential energy and energy gradients at each time step of the trajectories on the singlet and triplet ground electronic states using the UB3LYP density functional theory (DFT) with the 6-31G(d,p) basis set. We also have assessed the accuracy of the UB3LYP/6-31G(d,p) surfaces by comparing with the higher level of theory, such as CCSD(T), and found that the relative importance of the UB3LYP surfaces describing the $O(^3P,^1D) + H_2SO_4$ reaction is reasonably accurate. In addition, to describe intersystem crossing (ISC), we use a simplified version of the trajectory surface hopping (TSH) method. A decision to hop is made on the basis of the Tully's fewest switches method.[54] We have computed the spin-orbit coupling (SOC) matrix elements using GAMESS[55] with the Breit–Pauli method as implemented by Fedorov and Gordon.[56]

Supplementary Table 1. Electronic energies at various levels of calculations. The calculated total electronic energies (E_{total}), zero point vibrational energy (ZPE) corrected total electronic energies [E_{total} (ZPE)] of atomic oxygen, molecular oxygen, isolated molecules, isolated radicals, adducts, complexes, product molecules and transition states (TSs) at the M06-2X level in conjunction with the aug-cc-pVDZ and aug-cc-pVTZ basis sets, as well as at the CCSD(T)/aug-cc-pVTZ level of theory. The values given in the first bracket correspond to the ZPE corrected total electronic energies. The ZPE corrections in case of CCSD(T)/aug-cc-pVTZ level of calculations has been done from the M06-2X/aug-cc-pVTZ level predicted ZPE corrections.

Molecules/Complexes/ Adducts/Products/ Transition States	**M06-2X/ aug-cc-pVDZ**	**M06-2X/ aug-cc-pVTZ**	**CCSD(T)/ aug-cc-pVTZ**
$O(^1D)$	-74.9533329	-74.9708982	-74.89795
$O_2(^1\Delta_g)$	-150.2326093 (-150.228566)	-150.2657285 (-150.261733)	-150.0917833 (-150.0877883)
H_2SO_4	-700.142899 (-700.103764)	-700.28369 (-700.243859)	-699.4651536 (-699.4253226)
HSO_4	-699.453881 (-699.428288)	-699.5934209 (-699.566990)	-698.7782169 (-698.7517869)
OH	-75.7144248 (-75.705915)	-75.7337908 (-75.725248)	-75.6455845 (-75.6370415)
H_2O_2	-151.5152589 (-151.488077)	-151.5518609 (-151.525415)	-151.3736051 (-151.3471591)
H_2O	-76.4086225 (-76.387076)	-76.4300923 (-76.408534)	-76.3422892 (-76.3207312)
SO_3	-623.6959213 (-623.683909)	-623.8105923 (-623.797984)	-623.0876567 (-623.0750487)
SO_4	-698.7812767 (-698.765732)	-698.9190361 (-698.902763)	-698.1054834 (-698.0892104)
SO_2	-548.5380099 (-548.531032)	-548.6194445 (-548.612179)	-547.9900518 (-547.9827858)
H_2SO_4–$O(^1D)$ ≡ Ad-I	-775.1594444 (-775.117488)	-775.3142964 (-775.271737)	-774.4064827 (-774.3639237)
H_2SO_4–$O(^1D)$ ≡ Ad-II	-775.1920069 (-775.149746)	-775.3472206 (-775.304114)	-774.4406307 (-774.3975237)
$[H_2SO_4$–$O(^1D)]_{IIA}$ ≡ Ad-IIA	-775.1897605 (-775.147003)	-775.3451862 (-775.301907)	-774.4391842 (-774.3959052)
H_2SO_5–I	-775.2476345 (-775.204739)	-775.403418 (-775.359917)	-774.4942519 (-774.4507509)
H_2SO_5–II	-775.2520028 (-775.208952)	-775.40769991 (-775.364099)	-774.498472 (-774.454872)
$SO_3\cdots H_2O_2$	-775.229733 (-775.187129)	-775.383872 (-775.340569)	-774.4757609 (-774.4324579)
$(SO_3\cdots H_2O_2)^a$	-775.2297854	-775.3838672	-774.4777621

	(-775.187210)	(-775.340491)	(-774.4343861)
$SO_4^{\cdots}H_2O$	-775.2034497 (-775.163494)	-775.3617975 (-775.321291)	-774.4592487 (-774.4187417)
TS-I (Ad-I → H_2SO_5–I)	-775.1469799 (-775.108576)	-775.3027904 (-775.263811))	-774.3978283 (-774.3588453)
TS-IA (Ad–I → $SO_3^{\cdots}H_2O_2$)	-775.158322 (-775.116700)	-775.312633 (-775.270488)	-774.4044512 (-774.3623062)
TS-II (Ad-II → H_2SO_5–I)	-775.183391 (-775.143240)	-775.3392545 (-775.298338)	-774.4321035 (-774.3911865)
TS-III (H_2SO_5–II → $SO_3^{\cdots}H_2O_2$)	-775.192446 (-775.154171)	-775.3450292 (-775.306202)	-774.4374724 (-774.3986454)
TS-IV (Ad-II → Ad-IIA)	-775.1796054 (-775.138361)	-775.3345182 (-775.292713)	-774.427748 (-774.385943)
TS-V (Ad-IIA → $SO_4^{\cdots}H_2O$)	-775.1550841 (-775.117066)	-775.3102291 (-775.271379)	-774.4043994 (-774.3655484)
TS-VI (Ad-IIA → H_2SO_5–II)	-774.1220741 (-775.081609)	-775.2797799 (-775.238681)	-774.3998511 (-774.3587521)
TS-VII (H_2SO_5–I → H_2SO_5–II)	-775.2427484 (-775.200099)	-775.3979823 (-775.354975)	-774.4888465 (-774.4458392)

[a] $SO_3^{\cdots}H_2O_2$ product complex involved in the Ad–I → $SO_3^{\cdots}H_2O_2$ unimolecular reaction step via transition state TS-IA.

Supplementary Table 2. Imaginary frequencies. The imaginary frequencies (cm^{-1}) of various transition states at the M06-2X/aug-cc-pVDZ and M06-2X/aug-cc-pVTZ levels of calculations.

Transition States	**M06-2X/aug-cc-pVDZ**	**M06-2X/aug-cc-pVTZ**
TS-I (Ad-I $\rightarrow$ H_2SO_5–I)	-1232.2546	-1212.5320
TS-IA (Ad–I $\rightarrow$ SO_3···H_2O_2)	-82.5593	-96.6193
TS-II (Ad-II $\rightarrow$ H_2SO_5–I)	-351.8292	-328.5945
TS-III (H_2SO_5–II $\rightarrow$ SO_3···H_2O_2)	-1568.2231	-1587.0728
TS-IV (Ad-II $\rightarrow$ Ad-IIA)	-391.5171	-364.3538
TS-V (Ad-IIA $\rightarrow$ SO_4···H_2O)	-1542.5778	-1535.4381
TS-VI (Ad-IIA $\rightarrow$ H_2SO_5–II)	-796.1705	-809.9000
TS-VII (H_2SO_5–I $\rightarrow$ H_2SO_5–II)	-108.0598	-117.7209

Supplementary Table 3. T_1 diagnostic values. The T_1 diagnostic values for various species involved in the **Supplementary Figure 1** at the CCSD(T)/aug-cc-pVTZ level of calculations.

Atoms/Molecules/Adducts/ Complexes/Products/ Transition States	T_1 **Diagnostic**
$O(^1D)$	0.0058
$O_2(^1\Delta_g)$	0.0147
H_2SO_4	0.0154
HSO_4	0.0241
OH	0.0100
H_2O_2	0.0122
H_2O	0.0100
SO_3	0.0183
SO_4	0.0174
SO_2	0.0211
H_2SO_4–$O(^1D)$ ≡ Ad-I	0.0187
H_2SO_4–$O(^1D)$ ≡ Ad-II	0.0164
$[H_2SO_4$–$O(^1D)]_{IIA}$ ≡ Ad-IIA	0.0162
H_2SO_5–I	0.0160
H_2SO_5–II	0.0161
$SO_3\cdots H_2O_2$	0.0161
$SO_3\cdots H_2O_2$ [a]	0.0165
$SO_4\cdots H_2O$	0.0162
TS-I (Ad-I → H_2SO_5–I)	0.0217
TS-IA (Ad-I → $SO_3\cdots H_2O_2$)	0.0191
TS-II (Ad-II → H_2SO_5–I)	0.0189
TS-III (H_2SO_5–II → $SO_3\cdots H_2O_2$)	0.0173
TS-IV (Ad-II → Ad-IIA)	0.0167
TS-V (Ad-IIA → $SO_4\cdots H_2O$)	0.0165
TS-VI (Ad-IIA → H_2SO_5–II)	0.0298
TS-VII (H_2SO_5–I → H_2SO_5–II)	0.0163

[a] $SO_3\cdots H_2O_2$ product complex involved in the Ad–I → $SO_3\cdots H_2O_2$ unimolecular reaction step via transition state TS-IA.

Supplementary Table 4. Electronic energies at the CASPT2 level of calculations. The zero point vibrational energy (ZPE) corrected total electronic energies and approximate descriptions of active space for isolated atom, molecules and products associated with the TS-I in *Channel-I* (**a**) and Ad-IIA→ HSO_4···OH unimolecular reaction step via transition state TS-VIA (**b**) at the CASPT2(12,12)/aug-cc-pVDZ and CASPT2(12,12)/aug-cc-pVTZ levels of calculations. The description of active space used in the scan calculations have also been given in (**c**).

(a) H_2SO_4 (6,6) + $O(^1D)$ (6,6) ⇌ H_2SO_4–$O(^1D)$ [Ad-I] (12,12) → TS-I (12,12) → H_2SO_5-I (12,12)			
Species	**CASPT2 (12,12)/aug-cc-pVDZ**	**CASPT2 (12,12)/aug-cc-pVTZ**	**Active Space Description**
H_2SO_4 (6,6)	-699.0147011	-699.3680967	Bonding and Anti-bonding of (S–O)-σ, (O–H)-σ, (S–O)-O (non-bonding) orbitals
$O(^1D)$ (6,6)	-74.833180	-74.88745369	Bonding and Anti-bonding of *2s* and two *p* orbitals
H_2SO_4–$O(^1D)$ [Ad-I] (12,12)	-773.8866135	-774.2924861	Bonding and Anti-bonding of (S–O)-σ, (O–O)-σ, (O–H)-σ, (S–O)-O (non-bonding), $O(^1D)$-*p* orbitals.
TS-I (12,12)	-773.8822579	-774.2890962	Bonding and Anti-bonding of (S–O)-σ, (O–O)-σ, (O–H)-σ, (S–O)-O (non-bonding), $O(^1D)$-*p* orbitals.
H_2SO_5-I (12,12)	-773.9707278	-774.3770278	Bonding and Anti-bonding of (S=O)-σ, two (S=O)-O (non-bonding), (S=O)-π, (O–O)-σ, (O–H)-σ orbitals.
(b) H_2SO_4–$O(^1D)$ [Ad-IIA] (12,12) → TS-VIA (12,12) → HSO_4···OH (12,12)			
H_2SO_4–$O(^1D)$ [Ad-IIA] (12,12)	-773.9105569	-774.3213621	Bonding and Anti-bonding of three (S–O)-σ, (O–O)-σ, two (S–O)-O (non-bonding) plus (O–H)-σ mixed orbitals.
TS-VIA (12,12)	-773.8855438	-774.2927717	Bonding and Anti-bonding of three (S–O)-σ, (O–O)-σ, two (S–O)-O (non-bonding) plus (O–H)-σ mixed orbitals.
HSO_4···OH (12,12)	-773.9098602	-774.3191351	Bonding and Anti-bonding of (S=O)-π, two (S=O)-σ, (S–O)-O (non-bonding), (O–H)-σ orbitals and two SOMO.
(c) Description of (12,12) active space used for the scan calculations (see Supplementary Fig. 4)			
H_2SO_4–$O(^1D)$ [Ad-I] (O–O) Bond Scan			Bonding and Anti-bonding of (O–O)-σ, (O–H)-σ, (S–O)-σ, (S–O)-O (non-bonding), $O(^1D)$-*p* orbitals.
H_2SO_4–$O(^1D)$ [Ad-II] (O–O) Bond Scan			Bonding and Anti-bonding of (O–O)-σ, five mixed (S=O)/(S–O)-σ orbitals.
H_2SO_4–$O(^1D)$ [Ad-II] (S–O) Bond Scan			Bonding and Anti-bonding of (O–O)-σ, (S=O)-σ, two (S–O)-σ, (S=O)-π, (S=O)-O (non bonding) orbitals.

Supplementary Table 5. Variation of rate constants with respect to different sets of pivot points for *Channel–I*. The VRC-VTST predicted association rate constants (1×10^{-10} cm^3 $molecule^{-1}$ s^{-1}) for the formation of H_2SO_4–$O(^1D)$ (≡ Ad-I) adduct intermediate via *Channel–I* in the temperature range from 100K to 400K at different sets of pivot points. The calculations have been performed at the M06-2X/6-31G* level in the formalism of E,J-μVT. The configurations of pivot points have also been mentioned in the Table.

T(K)	Pivot point specifications					
	0.25Å above and below the O atom of OH bond	0.50Å above and below the O atom of OH bond	1.00Å above and below the O atom of OH bond	1.25Å above and below the O atom of OH bond	1.50Å above and below the O atom of OH bond	1.75Å above and below the O atom of OH bond
400	2.80	2.63	2.41	2.40	2.41	2.48
390	2.81	2.63	2.41	2.40	2.41	2.47
380	2.81	2.64	2.41	2.40	2.41	2.47
370	2.82	2.64	2.41	2.40	2.41	2.47
360	2.83	2.64	2.41	2.40	2.40	2.46
350	2.84	2.64	2.41	2.40	2.40	2.46
340	2.85	2.65	2.41	2.40	2.40	2.45
330	2.86	2.65	2.41	2.40	2.39	2.44
320	2.87	2.65	2.41	2.40	2.39	2.44
310	2.89	2.66	2.41	2.41	2.38	2.43
300	2.90	2.66	2.41	2.41	2.38	2.43
290	2.92	2.67	2.41	2.41	2.38	2.42
280	2.94	2.68	2.41	2.42	2.37	2.42
270	2.96	2.69	2.42	2.42	2.37	2.42
260	2.99	2.70	2.42	2.42	2.37	2.41
250	3.02	2.72	2.42	2.43	2.36	2.41
240	3.05	2.73	2.43	2.43	2.36	2.41
230	3.09	2.76	2.43	2.44	2.36	2.41
220	3.14	2.78	2.44	2.45	2.36	2.41
210	3.20	2.82	2.45	2.46	2.36	2.41
200	3.26	2.85	2.47	2.47	2.37	2.42
190	3.34	2.90	2.49	2.49	2.37	2.42
180	3.43	2.96	2.51	2.51	2.38	2.43
170	3.53	3.03	2.55	2.54	2.40	2.45
160	3.66	3.11	2.59	2.57	2.42	2.48
150	3.82	3.21	2.64	2.62	2.45	2.51
140	4.01	3.33	2.70	2.68	2.49	2.55
130	4.24	3.48	2.78	2.75	2.54	2.60
120	4.54	3.67	2.88	2.84	2.60	2.67
110	4.91	3.92	3.01	2.96	2.69	2.76
100	5.40	4.24	3.19	3.13	2.81	2.88

Supplementary Table 6. Variation of rate constants with respect to different sets of pivot points for *Channel–II*. The VRC-VTST predicted association rate constants (1×10^{-10} cm^3 $molecule^{-1}$ s^{-1}) for the formation of H_2SO_4–$O(^1D)$ (≡ Ad-II) adduct intermediate via *Channel–II* in the temperature range from 100K to 400K at different sets of pivot points. The calculations have been performed at the M06-2X/6-31G* level in the formalism of E,J-μVT. The configurations of pivot points have also been mentioned in the Table.

T(K)	Pivot point specifications						
	0.25Å above and below the O atom of S=O bond	0.50Å above and below the O atom of S=O bond	1.00Å above and below the O atom of S=O bond	1.25Å above and below the O atom of S=O bond	1.50Å above and below the O atom of S=O bond	1.75Å above and below the O atom of S=O bond	2.00Å above and below the O atom of S=O bond
400	3.22	2.86	2.53	2.43	2.38	2.39	2.43
390	3.23	2.86	2.52	2.42	2.37	2.38	2.42
380	3.25	2.87	2.52	2.41	2.36	2.38	2.41
370	3.26	2.87	2.51	2.41	2.35	2.37	2.41
360	3.28	2.88	2.51	2.40	2.34	2.36	2.39
350	3.30	2.89	2.50	2.39	2.33	2.35	2.38
340	3.32	2.90	2.50	2.38	2.32	2.33	2.38
330	3.34	2.91	2.49	2.37	2.31	2.33	2.37
320	3.37	2.92	2.49	2.37	2.31	2.32	2.36
310	3.39	2.93	2.48	2.36	2.30	2.31	2.35
300	3.43	2.94	2.48	2.35	2.29	2.30	2.34
290	3.46	2.96	2.48	2.35	2.29	2.29	2.34
280	3.50	2.98	2.48	2.34	2.28	2.29	2.33
270	3.55	3.00	2.48	2.34	2.27	2.28	2.32
260	3.60	3.02	2.48	2.33	2.26	2.27	2.31
250	3.66	3.05	2.48	2.33	2.26	2.26	2.30
240	3.72	3.08	2.48	2.33	2.25	2.25	2.30
230	3.80	3.12	2.49	2.32	2.25	2.25	2.29
220	3.89	3.17	2.49	2.32	2.24	2.24	2.29
210	3.99	3.23	2.50	2.32	2.24	2.24	2.28
200	4.11	3.29	2.52	2.33	2.23	2.23	2.28
190	4.24	3.36	2.53	2.33	2.23	2.23	2.27
180	4.40	3.45	2.56	2.34	2.24	2.23	2.27
170	4.59	3.56	2.58	2.35	2.24	2.23	2.27
160	4.82	3.69	2.62	2.37	2.25	2.23	2.28
150	5.09	3.84	2.67	2.39	2.27	2.24	2.29
140	5.42	4.02	2.73	2.42	2.29	2.25	2.30
130	5.83	4.25	2.80	2.46	2.32	2.27	2.32
120	6.34	4.55	2.90	2.52	2.36	2.30	2.35
110	6.99	4.92	3.03	2.59	2.41	2.35	2.39
100	7.83	5.41	3.20	2.69	2.49	2.40	2.46

Supplementary Table 7. Variation of rate constants with respect to different sets of pivot points for *Channel–III*. The VRC-VTST predicted association rate constants (1×10^{-10} cm^3 $molecule^{-1}$ s^{-1}) for the formation of H_2SO_5–II via *Channel–III* in the temperature range from 100K to 400K at different sets of pivot points. The calculations have been performed at the M06-2X/6-31G* level in the formalism of E,J-μVT. The configurations of pivot points have also been mentioned in the Table.

	Pivot point specifications			
T(K)	0.25Å above and below the S atom	0.50Å above and below the S atom	1.00Å above and below the S atom	1.25Å above and below the S atom
400	2.14	2.09	2.11	2.15
390	2.13	2.09	2.10	2.14
380	2.13	2.09	2.10	2.14
370	2.13	2.08	2.09	2.13
360	2.12	2.07	2.08	2.12
350	2.11	2.06	2.07	2.11
340	2.10	2.05	2.06	2.10
330	2.10	2.05	2.06	2.10
320	2.10	2.05	2.05	2.09
310	2.09	2.04	2.04	2.08
300	2.09	2.04	2.04	2.08
290	2.09	2.03	2.03	2.07
280	2.09	2.03	2.02	2.07
270	2.08	2.03	2.02	2.06
260	2.08	2.02	2.01	2.05
250	2.08	2.02	2.01	2.05
240	2.09	2.02	2.00	2.05
230	2.09	2.02	2.00	2.04
220	2.10	2.02	1.99	2.04
210	2.10	2.03	1.99	2.04
200	2.11	2.03	1.99	2.04
190	2.12	2.03	1.99	2.04
180	2.14	2.05	2.00	2.04
170	2.16	2.06	2.00	2.05
160	2.18	2.08	2.01	2.06
150	2.22	2.11	2.03	2.08
140	2.26	2.14	2.05	2.10
130	2.31	2.18	2.08	2.12
120	2.38	2.24	2.11	2.16
110	2.47	2.31	2.16	2.21
100	2.58	2.41	2.23	2.28

Supplementary Table 8. Rate constants and equilibrium constants associated with the first reaction steps. The VRC-VTST predicted minimized association rate constants (k_1) for the formation of H_2SO_4−$O(^1D)$ adduct intermediates (Ad-I and Ad-II) and H_2SO_5-II associated with the $O(^1D)$−initiated H_2SO_4 insertion reactions through the *Channel-I* to *III* at the M06-2X/6-31G* level of calculations with the formalism of E,J-μVT, and the equilibrium constants (K_{eq}) for the formation of Ad-I, Ad-II and H_2SO_5-II from the H_2SO_4 + $O(^1D)$ reactants according to the CCSD(T)/aug-cc-pVTZ level calculated energetics. The units of various rate constants and the decomposition rate constants (k_{-1}) for the decompositions of Ad-I, Ad-II and H_2SO_5-II into the H_2SO_4 + $O(^1D)$ reactants have also been given in the Table. The rate constants have been given in the temperature range from 100 to 400K with 10K interval. The electronic degeneracy of $O(^1D)$ = 5, but not the rotational symmetry number (σ = 2) of the most stable conformer of H_2SO_4, has been taken into account in predicting all the data presented in the Table.

T (K)	**k_1 (1×10^{-10} cm^3 molecule^{-1} sec^{-1})**			**K_{eq} (cm^3 molecule^{-1})**			**k_{-1} (sec^{-1}) ($k_{-1} = k_1/K_{eq}$)**		
	Channels			**H_2SO_4 + $O(^1D)$ ⇌ Ad-I**	**H_2SO_4 + $O(^1D)$ ⇌ Ad-II**	**H_2SO_4 + $O(^1D)$ ⇌ H_2SO_5–II**	**Ad-I → H_2SO_4 + $O(^1D)$**	**Ad-II → H_2SO_4 + $O(^1D)$**	**H_2SO_5–II → H_2SO_4 + $O(^1D)$**
	I	***II***	***III***						
400	2.40	2.38	2.09	2.28×10^{-12}	0.25	2.60×10^{19}	1.05×10^{2}	9.37×10^{-10}	8.04×10^{-30}
390	2.40	2.37	2.09	5.22×10^{-12}	1.15	3.74×10^{20}	4.60×10^{1}	2.06×10^{-10}	5.59×10^{-31}
380	2.40	2.36	2.09	1.24×10^{-11}	5.66	6.22×10^{21}	1.93×10^{1}	4.17×10^{-11}	3.36×10^{-32}
370	2.40	2.35	2.08	3.10×10^{-11}	30.4	1.20×10^{23}	7.74	7.73×10^{-12}	1.73×10^{-33}
360	2.40	2.34	2.07	8.14×10^{-11}	1.79×10^{2}	2.74×10^{24}	2.95	1.30×10^{-12}	7.55×10^{-35}
350	2.40	2.33	2.06	2.26×10^{-10}	1.17×10^{3}	7.46×10^{25}	1.06	1.99×10^{-13}	2.76×10^{-36}
340	2.40	2.32	2.05	6.68×10^{-10}	8.54×10^{3}	2.48×10^{27}	3.59×10^{-1}	2.72×10^{-14}	8.27×10^{-38}
330	2.39	2.31	2.05	2.12×10^{-9}	7.04×10^{4}	1.01×10^{29}	1.13×10^{-1}	3.28×10^{-15}	2.02×10^{-39}
320	2.39	2.31	2.05	7.16×10^{-9}	6.60×10^{5}	5.24×10^{30}	3.34×10^{-2}	3.50×10^{-16}	3.91×10^{-41}
310	2.38	2.30	2.04	2.64×10^{-8}	7.18×10^{6}	3.50×10^{32}	9.02×10^{-3}	3.20×10^{-17}	5.83×10^{-43}
300	2.38	2.29	2.04	1.05×10^{-7}	9.14×10^{7}	3.08×10^{34}	2.26×10^{-3}	2.51×10^{-18}	6.62×10^{-45}
290	2.38	2.29	2.03	4.66×10^{-7}	1.39×10^{9}	3.72×10^{36}	5.11×10^{-4}	1.65×10^{-19}	5.46×10^{-47}
280	2.37	2.28	2.02	2.28×10^{-6}	2.56×10^{10}	6.30×10^{38}	1.04×10^{-4}	8.91×10^{-21}	3.21×10^{-49}

270	2.37	2.27	2.02	1.26×10^{-5}	5.86×10^{11}	1.57×10^{41}	1.88×10^{-5}	3.87×10^{-22}	1.29×10^{-51}
260	2.37	2.26	2.01	7.98×10^{-5}	1.71×10^{13}	5.94×10^{43}	2.97×10^{-6}	1.32×10^{-23}	3.38×10^{-54}
250	2.36	2.26	2.01	5.84×10^{-4}	6.54×10^{14}	3.62×10^{46}	4.04×10^{-7}	3.46×10^{-25}	5.55×10^{-57}
240	2.36	2.25	2.00	5.04×10^{-3}	3.38×10^{16}	3.78×10^{49}	4.68×10^{-8}	6.66×10^{-27}	5.29×10^{-60}
230	2.36	2.25	2.00	5.26×10^{-2}	2.46×10^{18}	7.22×10^{52}	4.49×10^{-9}	9.15×10^{-29}	2.77×10^{-63}
220	2.36	2.24	1.99	6.78×10^{-1}	2.66×10^{20}	2.74×10^{56}	3.48×10^{-10}	8.42×10^{-31}	7.26×10^{-67}
210	2.36	2.24	1.99	1.12×10^{1}	4.46×10^{22}	2.28×10^{60}	2.11×10^{-11}	5.02×10^{-33}	8.73×10^{-71}
200	2.37	2.23	1.99	2.44×10^{2}	1.25×10^{25}	4.68×10^{64}	9.71×10^{-13}	1.78×10^{-35}	4.25×10^{-75}
190	2.37	2.23	1.99	7.36×10^{3}	6.34×10^{27}	2.74×10^{69}	3.22×10^{-14}	3.52×10^{-38}	7.26×10^{-80}
180	2.38	2.23	2.00	3.24×10^{5}	6.40×10^{30}	5.42×10^{74}	7.35×10^{-16}	3.48×10^{-41}	3.69×10^{-85}
170	2.40	2.23	2.00	2.24×10^{7}	1.46×10^{34}	4.50×10^{80}	1.07×10^{-17}	1.53×10^{-44}	4.44×10^{-91}
160	2.42	2.23	2.01	2.62×10^{9}	8.74×10^{37}	2.06×10^{87}	9.24×10^{-20}	2.55×10^{-48}	9.76×10^{-98}
150	2.45	2.24	2.03	5.76×10^{11}	1.66×10^{42}	7.26×10^{94}	4.25×10^{-22}	1.35×10^{-52}	2.80×10^{-105}
140	2.49	2.25	2.05	2.74×10^{14}	1.29×10^{47}	3.06×10^{103}	9.09×10^{-25}	1.74×10^{-57}	6.70×10^{-114}
130	2.54	2.27	2.08	3.38×10^{17}	5.62×10^{52}	2.74×10^{113}	7.51×10^{-28}	4.04×10^{-63}	7.59×10^{-124}
120	2.60	2.30	2.11	1.36×10^{21}	2.12×10^{59}	1.12×10^{125}	1.91×10^{-31}	1.08×10^{-69}	1.89×10^{-135}
110	2.69	2.35	2.16	2.26×10^{25}	1.25×10^{67}	5.86×10^{138}	1.09×10^{-35}	1.88×10^{-77}	3.69×10^{-149}
100	2.81	2.40	2.23	3.18×10^{30}	2.62×10^{76}	1.70×10^{155}	8.84×10^{-41}	9.16×10^{-87}	1.31×10^{-165}

Supplementary Table 9. Rate constants associated with various unimolecular steps. The CVT/SCT predicted rate constants (k_2) for the unimolecular steps associated with the Ad-I, Ad-II and H_2SO_5-II at the CCSD(T)/aug-cc-pVTZ level of theory. The rate constants have been given in the temperature range from 100 to 400K with 10K interval.

T (K)	k_2 (sec^{-1})				
	Ad-I → H_2SO_5–I	**(Ad-I → H_2SO_5–I)[a]**	**Ad-I → $SO_3\cdots H_2O_2$**	**Ad-II → H_2SO_5–I**	**H_2SO_5–II → $SO_3\cdots H_2O_2$**
400	2.72×10^{11}	6.08×10^{11}	8.33×10^{11}	4.50×10^{10}	2.81×10^{-6}
390	2.50×10^{11}	5.67×10^{11}	8.04×10^{11}	3.91×10^{10}	9.75×10^{-7}
380	2.28×10^{11}	5.28×10^{11}	7.76×10^{11}	3.38×10^{10}	3.22×10^{-7}
370	2.08×10^{11}	4.90×10^{11}	7.46×10^{11}	2.89×10^{10}	1.01×10^{-7}
360	1.89×10^{11}	4.53×10^{11}	7.17×10^{11}	2.46×10^{10}	2.98×10^{-8}
350	1.71×10^{11}	4.19×10^{11}	6.87×10^{11}	2.07×10^{10}	8.35×10^{-9}
340	1.54×10^{11}	3.85×10^{11}	6.57×10^{11}	1.72×10^{10}	2.22×10^{-9}
330	1.39×10^{11}	3.54×10^{11}	6.27×10^{11}	1.42×10^{10}	5.61×10^{-10}
320	1.24×10^{11}	3.24×10^{11}	5.97×10^{11}	1.16×10^{10}	1.38×10^{-10}
310	1.11×10^{11}	2.95×10^{11}	5.66×10^{11}	9.32×10^{9}	3.43×10^{-11}
300	9.89×10^{10}	2.69×10^{11}	5.35×10^{11}	7.39×10^{9}	9.00×10^{-12}
290	8.76×10^{10}	2.44×10^{11}	5.04×10^{11}	5.78×10^{9}	2.59×10^{-12}
280	7.74×10^{10}	2.20×10^{11}	4.74×10^{11}	4.44×10^{9}	8.10×10^{-13}
270	6.81×10^{10}	1.98×10^{11}	4.43×10^{11}	3.35×10^{9}	2.62×10^{-13}
260	5.97×10^{10}	1.78×10^{11}	4.12×10^{11}	2.48×10^{9}	8.35×10^{-14}
250	5.21×10^{10}	1.59×10^{11}	3.82×10^{11}	1.79×10^{9}	2.52×10^{-14}
240	4.54×10^{10}	1.42×10^{11}	3.52×10^{11}	1.26×10^{9}	7.02×10^{-15}
230	3.94×10^{10}	1.26×10^{11}	3.22×10^{11}	8.61×10^{8}	1.77×10^{-15}
220	3.41×10^{10}	1.11×10^{11}	2.93×10^{11}	5.71×10^{8}	4.00×10^{-16}
210	2.94×10^{10}	9.83×10^{10}	2.64×10^{11}	3.65×10^{8}	7.88×10^{-17}
200	2.53×10^{10}	8.64×10^{10}	2.36×10^{11}	2.24×10^{8}	1.33×10^{-17}
190	2.17×10^{10}	7.56×10^{10}	2.09×10^{11}	1.32×10^{8}	1.88×10^{-18}
180	1.87×10^{10}	6.61×10^{10}	1.83×10^{11}	7.38×10^{7}	2.16×10^{-19}
170	1.60×10^{10}	5.75×10^{10}	1.58×10^{11}	3.92×10^{7}	1.93×10^{-20}
160	1.37×10^{10}	4.99×10^{10}	1.34×10^{11}	1.97×10^{7}	1.29×10^{-21}
150	1.17×10^{10}	4.32×10^{10}	1.12×10^{11}	9.52×10^{6}	6.08×10^{-23}
140	9.99×10^{9}	3.72×10^{10}	9.19×10^{10}	4.54×10^{6}	1.87×10^{-24}
130	8.52×10^{9}	3.20×10^{10}	7.35×10^{10}	2.27×10^{6}	3.40×10^{-26}
120	7.25×10^{9}	2.74×10^{10}	5.72×10^{10}	1.28×10^{6}	3.22×10^{-28}
110	6.15×10^{9}	2.34×10^{10}	4.30×10^{10}	8.52×10^{5}	1.32×10^{-30}
100	5.19×10^{9}	1.98×10^{10}	3.11×10^{10}	6.35×10^{5}	1.85×10^{-33}

[a]The values given based on the CASPT2(12,12)/aug-cc-pVTZ level predicted energetics including ZPE correction at the M06-2X/aug-cc-pVTZ level of theory.

Supplementary Table 10. Pressure variation of VRC-VTST predicted rate constants for *Channel–I* by considering the reaction terminate in the first step. The Bartis-Widom phenomenological rate coefficients (k') or rate for the pseudo 1st order loss of $O(^1D)$ and extracted overall rate constants (k) associated with the formation of H_2SO_4–$O(^1D)$ (≡ Ad-I) adduct intermediate via *Channel–I* at atmospheric pressures and temperatures from 0 to 110 km altitudes of Earth's atmosphere. Atmospheric temperatures and pressures have been taken from Ref. 46. The concentration of H_2SO_4 (excess reactant in the MESMER run) has been taken from Ref. 43 and above 60 km altitude, the mixing ratios of H_2SO_4 by volume are assumed to be constant only for an understanding the pressure dependency of rate constants associated with exothermic reactions (see Supplementary Note-3). [a](Ref. 49).

Altitude (km)	P (atm)	T(K)	VRC-VTST rate constant (cm^3 $molecule^{-1}$ s^{-1})	Concentration of excess reactant (molecules cm^{-3})	Pseudo 1st order rate coefficient (k') of $O(^1D)$ loss (sec^{-1})	Extracted overall rate constants (k) (cm^3 $molecule^{-1}s^{-1}$)
0	1.0	298.15	2.38×10^{-10}	3.7×10^{8}	7.91×10^{-2}	2.14×10^{-10}
5	5.33×10^{-1}	256	2.36×10^{-10}	6.0×10^{7}	1.34×10^{-2}	2.23×10^{-10}
10	2.62×10^{-1}	223	2.36×10^{-10}	8.3×10^{6}	1.90×10^{-3}	2.29×10^{-10}
15	1.20×10^{-1}	217	2.36×10^{-10}	2.4×10^{5}	5.31×10^{-5}	2.21×10^{-10}
20	5.50×10^{-2}	217	2.36×10^{-10}	3.9×10^{4}	8.03×10^{-6}	2.06×10^{-10}
25	2.50×10^{-2}	222	2.36×10^{-10}	2.5×10^{5}	4.48×10^{-5}	1.79×10^{-10}
30	1.18×10^{-2}	227	2.36×10^{-10}	$(3.7\times10^{7})^{a}$	5.46×10^{-3}	1.48×10^{-10}
35	5.63×10^{-3}	237	2.36×10^{-10}	$(5.0\times10^{7})^{a}$	5.40×10^{-3}	1.08×10^{-10}
40	2.27×10^{-3}	250	2.36×10^{-10}	$(1.6\times10^{7})^{a}$	1.03×10^{-3}	6.44×10^{-11}
45	1.48×10^{-3}	264	2.37×10^{-10}	$(3.8\times10^{6})^{a}$	1.62×10^{-4}	4.26×10^{-11}
50	7.89×10^{-4}	271	2.37×10^{-10}	$(1.6\times10^{6})^{a}$	4.29×10^{-5}	2.68×10^{-11}
55	4.24×10^{-4}	261	2.37×10^{-10}	1.3×10^{6}	2.78×10^{-5}	2.14×10^{-11}
60	2.17×10^{-4}	247	2.36×10^{-10}	7.2×10^{5}	1.25×10^{-5}	1.74×10^{-11}
65	1.09×10^{-4}	233	2.36×10^{-10}	3.7×10^{5}	5.11×10^{-6}	1.38×10^{-11}
70	5.13×10^{-5}	220	2.36×10^{-10}	1.9×10^{5}	1.93×10^{-6}	1.02×10^{-11}
75	2.37×10^{-5}	208	2.36×10^{-10}	9.2×10^{4}	6.51×10^{-7}	7.08×10^{-12}
80	1.09×10^{-5}	198	2.37×10^{-10}	4.4×10^{4}	2.02×10^{-7}	4.59×10^{-12}
85	4.44×10^{-6}	189	2.37×10^{-10}	1.9×10^{4}	4.83×10^{-8}	2.54×10^{-12}
90	1.78×10^{-6}	187	2.38×10^{-10}	7.7×10^{3}	8.87×10^{-9}	1.15×10^{-12}
95	7.50×10^{-7}	188	2.38×10^{-10}	3.2×10^{3}	1.64×10^{-9}	5.13×10^{-13}
100	3.16×10^{-7}	195	2.37×10^{-10}	1.3×10^{3}	2.62×10^{-10}	2.02×10^{-13}
105	1.48×10^{-7}	209	2.36×10^{-10}	5.7×10^{2}	1.27×10^{-11}	2.23×10^{-14}
110	7.01×10^{-8}	240	2.36×10^{-10}	2.3×10^{2}	4.26×10^{-12}	1.85×10^{-14}

Supplementary Table 11. Pressure variation of VRC-VTST predicted rate constants for *Channel–II* by considering the reaction terminate in the first step. The Bartis-Widom phenomenological rate coefficients (k') or rate for the pseudo 1st order loss of $O(^1D)$ and extracted overall rate constants (k) associated with the formation of H_2SO_4–$O(^1D)$ (≡ Ad-II) adduct intermediate via *Channel–II* at atmospheric pressures and temperatures from 0 to 110 km altitudes of Earth's atmosphere. Atmospheric temperatures and pressures have been taken from Ref. 46. The concentration of H_2SO_4 (excess reactant in the MESMER run) has been taken from Ref. 43 and above 60 km altitude, the mixing ratios of H_2SO_4 by volume are assumed to be constant only for an understanding the pressure dependency of rate constants associated with exothermic reactions (see Supplementary Note-3). [a](Ref. 49).

Altitude (km)	P (atm)	T(K)	VRC-VTST rate constant (cm^3 $molecule^{-1}$ s^{-1})	Concentration of excess reactant (molecules cm^{-3})	Pseudo 1st order rate coefficient (k') of $O(^1D)$ loss (sec^{-1})	Extracted overall rate constants (k) (cm^3 $molecule^{-1}s^{-1}$)
0	1.0	298.15	2.29×10^{-10}	3.7×10^{8}	8.62×10^{-2}	2.33×10^{-10}
5	5.33×10^{-1}	256	2.26×10^{-10}	6.0×10^{7}	1.39×10^{-2}	2.32×10^{-10}
10	2.62×10^{-1}	223	2.24×10^{-10}	8.3×10^{6}	1.92×10^{-3}	2.31×10^{-10}
15	1.20×10^{-1}	217	2.24×10^{-10}	2.4×10^{5}	5.57×10^{-5}	2.32×10^{-10}
20	5.50×10^{-2}	217	2.24×10^{-10}	3.9×10^{4}	9.04×10^{-6}	2.32×10^{-10}
25	2.50×10^{-2}	222	2.24×10^{-10}	2.5×10^{5}	5.77×10^{-5}	2.31×10^{-10}
30	1.18×10^{-2}	227	2.24×10^{-10}	$(3.7\times10^{7})^{a}$	8.49×10^{-3}	2.29×10^{-10}
35	5.63×10^{-3}	237	2.25×10^{-10}	$(5.0\times10^{7})^{a}$	1.13×10^{-2}	2.26×10^{-10}
40	2.27×10^{-3}	250	2.26×10^{-10}	$(1.6\times10^{7})^{a}$	3.47×10^{-3}	2.17×10^{-10}
45	1.48×10^{-3}	264	2.26×10^{-10}	$(3.8\times10^{6})^{a}$	7.76×10^{-4}	2.04×10^{-10}
50	7.89×10^{-4}	271	2.27×10^{-10}	$(1.6\times10^{6})^{a}$	3.00×10^{-4}	1.88×10^{-10}
55	4.24×10^{-4}	261	2.26×10^{-10}	1.3×10^{6}	2.33×10^{-4}	1.79×10^{-10}
60	2.17×10^{-4}	247	2.25×10^{-10}	7.2×10^{5}	1.26×10^{-4}	1.75×10^{-10}
65	1.09×10^{-4}	233	2.25×10^{-10}	3.7×10^{5}	6.22×10^{-5}	1.68×10^{-10}
70	5.13×10^{-5}	220	2.24×10^{-10}	1.9×10^{5}	3.00×10^{-5}	1.58×10^{-10}
75	2.37×10^{-5}	208	2.23×10^{-10}	9.2×10^{4}	1.35×10^{-5}	1.47×10^{-10}
80	1.09×10^{-5}	198	2.23×10^{-10}	4.4×10^{4}	5.80×10^{-6}	1.32×10^{-10}
85	4.44×10^{-6}	189	2.23×10^{-10}	1.9×10^{4}	2.10×10^{-6}	1.11×10^{-10}
90	1.78×10^{-6}	187	2.23×10^{-10}	7.7×10^{3}	6.18×10^{-7}	8.03×10^{-11}
95	7.50×10^{-7}	188	2.23×10^{-10}	3.2×10^{3}	1.68×10^{-7}	5.25×10^{-11}
100	3.16×10^{-7}	195	2.23×10^{-10}	1.3×10^{3}	3.67×10^{-8}	2.82×10^{-11}
105	1.48×10^{-7}	209	2.23×10^{-10}	5.7×10^{2}	7.38×10^{-9}	1.29×10^{-11}
110	7.01×10^{-8}	240	2.25×10^{-10}	2.3×10^{2}	9.02×10^{-10}	3.92×10^{-12}

Supplementary Table 12. Pressure variation of VRC-VTST predicted rate constants for *Channel–III* by considering the reaction terminate in the first step. The Bartis-Widom phenomenological rate coefficients (k') or rate for the pseudo 1st order loss of $O(^1D)$ and extracted overall rate constants (k) associated with the formation of H_2SO_5–II via *Channel–III* at atmospheric pressures and temperatures from 0 to 110 km altitudes of Earth's atmosphere. Atmospheric temperatures and pressures have been taken from Ref. 46. The concentration of H_2SO_4 (excess reactant in the MESMER run) has been taken from Ref. 43 and above 60 km altitude, the mixing ratios of H_2SO_4 by volume are assumed to be constant only for an understanding the pressure dependency of rate constants associated with exothermic reactions (see Supplementary Note-3). [a](Ref. 49).

Altitude (km)	P (atm)	T(K)	VRC-VTST rate constant (cm^3 $molecule^{-1}$ s^{-1})	Concentration of excess reactant (molecules cm^{-3})	Pseudo 1st order rate coefficient (k') of $O(^1D)$ loss (sec^{-1})	Extracted overall rate constants (k) (cm^3 $molecule^{-1}s^{-1}$)
0	1.0	298.15	2.03×10^{-10}	3.7×10^{8}	7.69×10^{-2}	2.08×10^{-10}
5	5.33×10^{-1}	256	2.01×10^{-10}	6.0×10^{7}	1.24×10^{-2}	2.07×10^{-10}
10	2.62×10^{-1}	223	1.99×10^{-10}	8.3×10^{6}	1.72×10^{-3}	2.07×10^{-10}
15	1.20×10^{-1}	217	1.99×10^{-10}	2.4×10^{5}	4.98×10^{-5}	2.08×10^{-10}
20	5.50×10^{-2}	217	1.99×10^{-10}	3.9×10^{4}	8.09×10^{-6}	2.07×10^{-10}
25	2.50×10^{-2}	222	1.99×10^{-10}	2.5×10^{5}	5.18×10^{-5}	2.07×10^{-10}
30	1.18×10^{-2}	227	1.99×10^{-10}	$(3.7\times10^{7})^{a}$	7.65×10^{-3}	2.07×10^{-10}
35	5.63×10^{-3}	237	2.00×10^{-10}	$(5.0\times10^{7})^{a}$	1.04×10^{-2}	2.08×10^{-10}
40	2.27×10^{-3}	250	2.01×10^{-10}	$(1.6\times10^{7})^{a}$	3.32×10^{-3}	2.08×10^{-10}
45	1.48×10^{-3}	264	2.01×10^{-10}	$(3.8\times10^{6})^{a}$	7.86×10^{-4}	2.07×10^{-10}
50	7.89×10^{-4}	271	2.02×10^{-10}	$(1.6\times10^{6})^{a}$	3.32×10^{-4}	2.08×10^{-10}
55	4.24×10^{-4}	261	2.01×10^{-10}	1.3×10^{6}	2.70×10^{-4}	2.08×10^{-10}
60	2.17×10^{-4}	247	2.01×10^{-10}	7.2×10^{5}	1.49×10^{-4}	2.07×10^{-10}
65	1.09×10^{-4}	233	2.00×10^{-10}	3.7×10^{5}	7.67×10^{-5}	2.07×10^{-10}
70	5.13×10^{-5}	220	1.99×10^{-10}	1.9×10^{5}	3.94×10^{-5}	2.07×10^{-10}
75	2.37×10^{-5}	208	1.99×10^{-10}	9.2×10^{4}	1.91×10^{-5}	2.08×10^{-10}
80	1.09×10^{-5}	198	1.99×10^{-10}	4.4×10^{4}	9.20×10^{-6}	2.09×10^{-10}
85	4.44×10^{-6}	189	1.99×10^{-10}	1.9×10^{4}	3.98×10^{-6}	2.09×10^{-10}
90	1.78×10^{-6}	187	1.99×10^{-10}	7.7×10^{3}	1.61×10^{-6}	2.09×10^{-10}
95	7.50×10^{-7}	188	1.99×10^{-10}	3.2×10^{3}	6.68×10^{-7}	2.09×10^{-10}
100	3.16×10^{-7}	195	1.99×10^{-10}	1.3×10^{3}	2.67×10^{-7}	2.05×10^{-10}
105	1.48×10^{-7}	209	1.99×10^{-10}	5.7×10^{2}	1.12×10^{-7}	1.96×10^{-10}
110	7.01×10^{-8}	240	2.00×10^{-10}	2.3×10^{2}	3.94×10^{-8}	1.71×10^{-10}

Supplementary Table 13. Pressure variation of VRC-VTST predicted rate constants for *Channel–I* via TS-IA. The Bartis-Widom phenomenological rate coefficients (k') or rate for the pseudo 1st order loss of $O(^1D)$ and extracted overall rate constants (k) associated with the formation of $SO_3 + H_2O_2$ in *Channel–I* via TS-IA at atmospheric pressures and temperatures from 0 to 110 km altitudes of Earth's atmosphere. Atmospheric temperatures and pressures have been taken from Ref. 46. The concentration of H_2SO_4 (excess reactant in the MESMER run) has been taken from Ref. 43 and above 60 km altitude, the mixing ratios of H_2SO_4 by volume are assumed to be constant only for an understanding the pressure dependency of rate constants associated with exothermic reactions (see Supplementary Note-3). [a](Ref. 49).

Altitude (km)	P (atm)	T (Kelvin)	VRC-VTST rate constant (cm^3 $molecule^{-1}$ s^{-1})	Concentration of excess reactant (molecules cm^{-3})	Pseudo 1st order rate coefficient (k') of $O(^1D)$ loss (sec^{-1})	Extracted overall rate constants (k) (cm^3 $molecule^{-1}s^{-1}$)
0	1.0	298.15	2.38×10^{-10}	3.7×10^{8}	8.96×10^{-2}	2.42×10^{-10}
5	5.33×10^{-1}	256	2.36×10^{-10}	6.0×10^{7}	1.45×10^{-2}	2.42×10^{-10}
10	2.62×10^{-1}	223	2.36×10^{-10}	8.3×10^{6}	2.02×10^{-3}	2.43×10^{-10}
15	1.20×10^{-1}	217	2.36×10^{-10}	2.4×10^{5}	5.86×10^{-5}	2.44×10^{-10}
20	5.50×10^{-2}	217	2.36×10^{-10}	3.9×10^{4}	9.53×10^{-6}	2.44×10^{-10}
25	2.50×10^{-2}	222	2.36×10^{-10}	2.5×10^{5}	6.09×10^{-5}	2.44×10^{-10}
30	1.18×10^{-2}	227	2.36×10^{-10}	$(3.7\times10^{7})^{a}$	9.01×10^{-3}	2.44×10^{-10}
35	5.63×10^{-3}	237	2.36×10^{-10}	$(5.0\times10^{7})^{a}$	1.21×10^{-2}	2.42×10^{-10}
40	2.27×10^{-3}	250	2.36×10^{-10}	$(1.6\times10^{7})^{a}$	3.88×10^{-3}	2.43×10^{-10}
45	1.48×10^{-3}	264	2.37×10^{-10}	$(3.8\times10^{6})^{a}$	9.22×10^{-4}	2.43×10^{-10}
50	7.89×10^{-4}	271	2.37×10^{-10}	$(1.6\times10^{6})^{a}$	3.88×10^{-4}	2.43×10^{-10}
55	4.24×10^{-4}	261	2.37×10^{-10}	1.3×10^{6}	3.16×10^{-4}	2.43×10^{-10}
60	2.17×10^{-4}	247	2.36×10^{-10}	7.2×10^{5}	1.75×10^{-4}	2.43×10^{-10}
65	1.09×10^{-4}	233	2.36×10^{-10}	3.7×10^{5}	8.99×10^{-5}	2.43×10^{-10}
70	5.13×10^{-5}	220	2.36×10^{-10}	1.9×10^{5}	4.64×10^{-5}	2.44×10^{-10}
75	2.37×10^{-5}	208	2.36×10^{-10}	9.2×10^{4}	2.25×10^{-5}	2.45×10^{-10}
80	1.09×10^{-5}	198	2.37×10^{-10}	4.4×10^{4}	1.09×10^{-5}	2.48×10^{-10}
85	4.44×10^{-6}	189	2.37×10^{-10}	1.9×10^{4}	4.71×10^{-6}	2.48×10^{-10}
90	1.78×10^{-6}	187	2.38×10^{-10}	7.7×10^{3}	1.92×10^{-6}	2.49×10^{-10}
95	7.50×10^{-7}	188	2.38×10^{-10}	3.2×10^{3}	7.98×10^{-7}	2.49×10^{-10}
100	3.16×10^{-7}	195	2.37×10^{-10}	1.3×10^{3}	3.22×10^{-7}	2.48×10^{-10}
105	1.48×10^{-7}	209	2.36×10^{-10}	5.7×10^{2}	1.40×10^{-7}	2.46×10^{-10}
110	7.01×10^{-8}	240	2.36×10^{-10}	2.3×10^{2}	5.58×10^{-8}	2.43×10^{-10}

Supplementary Table S14. Pressure variation of VRC-VTST predicted rate constants for *Channel–II*. The Bartis-Widom phenomenological rate coefficients (k') or rate for the pseudo 1st order loss of $O(^1D)$ and extracted overall rate constants (k) associated with the formation of H_2SO_5–I via *Channel–II* at atmospheric pressures and temperatures from 0 to 110 km altitudes of Earth's atmosphere. Atmospheric temperatures and pressures have been taken from Ref. 46. The concentration of H_2SO_4 (excess reactant in the MESMER run) has been taken from Ref. 43 and above 60 km altitude, the mixing ratios of H_2SO_4 by volume are assumed to be constant only for an understanding the pressure dependency of rate constants associated with exothermic reactions (see Supplementary Note-3). [a](Ref. 49).

Altitude (km)	P (atm)	T(K)	VRC-VTST rate constant (cm^3 $molecule^{-1}$ s^{-1})	Concentration of excess reactant (molecules cm^{-3})	Pseudo 1st order rate coefficient (k') of $O(^1D)$ loss (sec^{-1})	Extracted overall rate constants (k) (cm^3 $molecule^{-1}$ s^{-1})
0	1.0	298.15	2.29×10^{-10}	3.7×10^{8}	8.63×10^{-2}	2.33×10^{-10}
5	5.33×10^{-1}	256	2.26×10^{-10}	6.0×10^{7}	1.39×10^{-2}	2.32×10^{-10}
10	2.62×10^{-1}	223	2.24×10^{-10}	8.3×10^{6}	1.90×10^{-3}	2.29×10^{-10}
15	1.20×10^{-1}	217	2.24×10^{-10}	2.4×10^{5}	5.57×10^{-5}	2.32×10^{-10}
20	5.50×10^{-2}	217	2.24×10^{-10}	3.9×10^{4}	9.06×10^{-6}	2.32×10^{-10}
25	2.50×10^{-2}	222	2.24×10^{-10}	2.5×10^{5}	5.80×10^{-5}	2.32×10^{-10}
30	1.18×10^{-2}	227	2.24×10^{-10}	$(3.7\times10^{7})^{a}$	8.56×10^{-3}	2.31×10^{-10}
35	5.63×10^{-3}	237	2.25×10^{-10}	$(5.0\times10^{7})^{a}$	1.16×10^{-2}	2.32×10^{-10}
40	2.27×10^{-3}	250	2.26×10^{-10}	$(1.6\times10^{7})^{a}$	3.72×10^{-3}	2.33×10^{-10}
45	1.48×10^{-3}	264	2.26×10^{-10}	$(3.8\times10^{6})^{a}$	8.79×10^{-4}	2.31×10^{-10}
50	7.89×10^{-4}	271	2.27×10^{-10}	$(1.6\times10^{6})^{a}$	3.72×10^{-4}	2.33×10^{-10}
55	4.24×10^{-4}	261	2.26×10^{-10}	1.3×10^{6}	3.01×10^{-4}	2.32×10^{-10}
60	2.17×10^{-4}	247	2.25×10^{-10}	7.2×10^{5}	1.67×10^{-4}	2.32×10^{-10}
65	1.09×10^{-4}	233	2.25×10^{-10}	3.7×10^{5}	8.59×10^{-5}	2.32×10^{-10}
70	5.13×10^{-5}	220	2.24×10^{-10}	1.9×10^{5}	4.41×10^{-5}	2.32×10^{-10}
75	2.37×10^{-5}	208	2.23×10^{-10}	9.2×10^{4}	2.13×10^{-5}	2.32×10^{-10}
80	1.09×10^{-5}	198	2.23×10^{-10}	4.4×10^{4}	1.02×10^{-5}	2.32×10^{-10}
85	4.44×10^{-6}	189	2.23×10^{-10}	1.9×10^{4}	4.44×10^{-6}	2.34×10^{-10}
90	1.78×10^{-6}	187	2.23×10^{-10}	7.7×10^{3}	1.80×10^{-6}	2.34×10^{-10}
95	7.50×10^{-7}	188	2.23×10^{-10}	3.2×10^{3}	7.49×10^{-7}	2.34×10^{-10}
100	3.16×10^{-7}	195	2.23×10^{-10}	1.3×10^{3}	3.03×10^{-7}	2.33×10^{-10}
105	1.48×10^{-7}	209	2.23×10^{-10}	5.7×10^{2}	1.32×10^{-7}	2.32×10^{-10}
110	7.01×10^{-8}	240	2.25×10^{-10}	2.3×10^{2}	5.28×10^{-8}	2.30×10^{-10}

Supplementary Table 15. Pressure variation of VRC-VTST predicted rate constants for *Channel–III*. The Bartis-Widom phenomenological rate coefficients (k') or rate for the pseudo 1st order loss of $O(^1D)$ and extracted overall rate constants (k) associated with the formation of $SO_3 + H_2O_2$ via *Channel–III* at atmospheric pressures and temperatures from 0 to 110 km altitudes of Earth's atmosphere. Atmospheric temperatures and pressures have been taken from Ref. 46. The concentration of H_2SO_4 (excess reactant in the MESMER run) has been taken from Ref. 43 and above 60 km altitude, the mixing ratios of H_2SO_4 by volume are assumed to be constant only for an understanding the pressure dependency of rate constants associated with exothermic reactions (see Supplementary Note-3). [a](Ref. 49).

Altitude (km)	P (atm)	T(K)	VRC-VTST rate constant (cm^3 $molecule^{-1}$ s^{-1})	Concentration of excess reactant (molecules cm^{-3})	Pseudo 1st order rate coefficient (k') of $O(^1D)$ loss (sec^{-1})	Extracted overall rate constants (k) (cm^3 $molecule^{-1}$ s^{-1})
0	1.0	298.15	2.03×10^{-10}	3.7×10^{8}	7.69×10^{-2}	2.08×10^{-10}
5	5.33×10^{-1}	256	2.01×10^{-10}	6.0×10^{7}	1.24×10^{-2}	2.07×10^{-10}
10	2.62×10^{-1}	223	1.99×10^{-10}	8.3×10^{6}	1.72×10^{-3}	2.07×10^{-10}
15	1.20×10^{-1}	217	1.99×10^{-10}	2.4×10^{5}	4.98×10^{-5}	2.08×10^{-10}
20	5.50×10^{-2}	217	1.99×10^{-10}	3.9×10^{4}	8.09×10^{-6}	2.07×10^{-10}
25	2.50×10^{-2}	222	1.99×10^{-10}	2.5×10^{5}	5.18×10^{-5}	2.07×10^{-10}
30	1.18×10^{-2}	227	1.99×10^{-10}	$(3.7\times10^{7})^{a}$	7.65×10^{-3}	2.07×10^{-10}
35	5.63×10^{-3}	237	2.00×10^{-10}	$(5.0\times10^{7})^{a}$	1.04×10^{-2}	2.08×10^{-10}
40	2.27×10^{-3}	250	2.01×10^{-10}	$(1.6\times10^{7})^{a}$	3.32×10^{-3}	2.08×10^{-10}
45	1.48×10^{-3}	264	2.01×10^{-10}	$(3.8\times10^{6})^{a}$	7.86×10^{-4}	2.07×10^{-10}
50	7.89×10^{-4}	271	2.02×10^{-10}	$(1.6\times10^{6})^{a}$	3.32×10^{-4}	2.08×10^{-10}
55	4.24×10^{-4}	261	2.01×10^{-10}	1.3×10^{6}	2.69×10^{-4}	2.07×10^{-10}
60	2.17×10^{-4}	247	2.01×10^{-10}	7.2×10^{5}	1.50×10^{-4}	2.08×10^{-10}
65	1.09×10^{-4}	233	2.00×10^{-10}	3.7×10^{5}	7.68×10^{-5}	2.08×10^{-10}
70	5.13×10^{-5}	220	1.99×10^{-10}	1.9×10^{5}	3.94×10^{-5}	2.07×10^{-10}
75	2.37×10^{-5}	208	1.99×10^{-10}	9.2×10^{4}	1.92×10^{-5}	2.09×10^{-10}
80	1.09×10^{-5}	198	1.99×10^{-10}	4.4×10^{4}	9.20×10^{-6}	2.09×10^{-10}
85	4.44×10^{-6}	189	1.99×10^{-10}	1.9×10^{4}	4.00×10^{-6}	2.11×10^{-10}
90	1.78×10^{-6}	187	1.99×10^{-10}	7.7×10^{3}	1.62×10^{-6}	2.10×10^{-10}
95	7.50×10^{-7}	188	1.99×10^{-10}	3.2×10^{3}	6.73×10^{-7}	2.10×10^{-10}
100	3.16×10^{-7}	195	1.99×10^{-10}	1.3×10^{3}	2.72×10^{-7}	2.09×10^{-10}
105	1.48×10^{-7}	209	1.99×10^{-10}	5.7×10^{2}	1.19×10^{-7}	2.09×10^{-10}
110	7.01×10^{-8}	240	2.00×10^{-10}	2.3×10^{2}	4.76×10^{-8}	2.07×10^{-10}

Supplementary Table 16: The calculated rate constants and relative rates. The VRC-VTST predicted rate constants or overall rate constants (k_1=k) for the formation of H_2SO_5 (H_2SO_5-I and H_2SO_5-II) or SO_3 + H_2O_2 molecules in the *Channel-I* to *III*, corrected *J* values for visible photolysis derived from the different photolysis quantum yields (in%) at different altitudes [Ref. 47], *J* values derived from the experimentally measured overtone cross-sections (30 to 50 km altitude) with the assumption of quantum yield = 1 at all wavelengths [Ref. 48], *J* values due to UV photolysis [Ref. 49] using empirically derived UV absorption cross sections of 10^{-21} cm^2 $molecule^{-1}$ (upper limit) between 179 and 226 nm, theoretically predicted *J* values for both for UV and Lyman−α radiation in the 60-100 km altitude [Ref. 51], and the rate of insertion/addition reactions (*Channel-I* to *III*) with respect to the various above mentioned light induced H_2SO_4 photolysis or photo-dissociation reactions ($\nu_{Insertion}/\nu_{Photolysis}$) at various atmospheric pressures and temperatures corresponding to 30 to 110 km altitudes of Earth's atmosphere. To estimate the relative rates, we have considered the reaction degeneracy (σ) = 2 and 20% steady state concentration of $O(^1D)$ (see Supplementary Note-4 and Main Article). *J* values derived from the experimentally measured overtone cross-sections (30 to 50 km altitude) with the assumption of quantum yield = 1 at all wavelengths and corresponding $\nu_{Insertion}/\nu_{Photolysis}$ values have been given within the third brackets. Theoretically predicted *J* values both for UV and Lyman−α radiation in the 60-100 km altitude and corresponding $\nu_{Insertion}/\nu_{Photolysis}$ values have been given within the first (UV) and second brackets (Lyman−α radiation), respectively. *J* values for absorption of Lyman−α radiation above 100 km altitude are not known and assumed to be constant above 100 km altitude (see Supplementary Note-4). Concentrations of $O(^1D)$ have been taken from Ref. 45-46. Atmospheric temperatures and pressures have been taken from Ref. 46.The concentrations of $O(^1D)$ at the 105 and 110 km altitudes of the Earth's atmosphere are not known exactly and hence, we use the concentrations at 104 and 108.4 km as the concentrations of 105 and 110 km altitudes. [a][Ref. 45].

Altitude (km)	T(K)	Pressure (atm)	$[O(^1D)]$ atoms/ cm^3	*Channel-I*	*Channel-II*	*Channel-III*	*J* values (sec^{-1})		$\frac{\nu_{Insertion}}{\nu_{Photolysis}}$	
				k_1=k	k_1=k	k_1=k				
				(1×10^{-10} $cm^3molecule^{-1}sec^{-1}$)			Derived UV or calculated	Visible or Lyman−α	UV	Visible or Lyman−α
30	227	1.18×10^{-2}	$(4.0\times10^{1})^{a}$	2.36	2.24	1.99	2.08×10^{-11}	5.3×10^{-9} [4.3×10^{-8}]	506.9	2 [0.2]
35	237	5.63×10^{-3}	$(1.0\times10^{2})^{a}$	2.36	2.25	2.00	3.24×10^{-10}	9.1×10^{-9} [4.6×10^{-8}]	81.6	2.9 [0.6]
40	250	2.27×10^{-3}	$(2.0\times10^{2})^{a}$	2.36	2.26	2.01	2.81×10^{-9}	1.4×10^{-8} [4.6×10^{-8}]	18.9	3.8 [1.2]
45	264	1.48×10^{-3}	$(3.0\times10^{2})^{a}$	2.37	2.26	2.01	1.08×10^{-8}	2.2×10^{-8}	7.4	3.6

								(4.6×10^{-8})		[1.7]
50	271	7.89×10^{-4}	(3.2×10^{2})[a]	2.37	2.27	2.02	2.21×10^{-8}	3.0×10^{-8} [4.9×10^{-8}]	3.9	2.8 [1.7]
55	261	4.24×10^{-4}	1.5×10^{2}	2.37	2.26	2.01	3.03×10^{-8}	3.8×10^{-8}	1.3	1
60	247	2.17×10^{-4}	1.1×10^{2}	2.36	2.25	2.01	3.59×10^{-8} (3.70×10^{-11})	4.7×10^{-8} {2.98×10^{-10}}	0.8 (787)	0.6 {97.8}
65	233	1.09×10^{-4}	7.5×10^{1}	2.36	2.25	2.00	3.95×10^{-8}	5.4×10^{-8}	0.5	0.4
70	220	5.13×10^{-5}	4.0×10^{1}	2.36	2.24	1.99	4.21×10^{-8} (1.11×10^{-10})	6.0×10^{-8} {3.91×10^{-7}}	0.3 (95)	0.2 {2.7×10^{-2}}
75	208	2.37×10^{-5}	1.9×10^{1}	2.36	2.23	1.99	4.41×10^{-8}	6.5×10^{-8}	0.1	0.1
80	198	1.09×10^{-5}	3.0×10^{1}	2.37	2.23	1.99	5.01×10^{-8} (2.39×10^{-10})	6.6×10^{-8} {3.90×10^{-6}}	0.2 (33)	0.1 {2×10^{-3}}
85	189	4.44×10^{-6}	1.2×10^{2}	2.37	2.23	1.99	---	---	---	---
90	187	1.78×10^{-6}	1.0×10^{2}	2.38	2.23	1.99	(8.40×10^{-10})	{7.20×10^{-6}}	(31.4)	{3.7×10^{-3}}
95	188	7.50×10^{-7}	2.0×10^{2}	2.38	2.23	1.99	---	---	---	---
100	195	3.16×10^{-7}	1.0×10^{3}	2.37	2.23	1.99	(1.01×10^{-8})	{8.87×10^{-6}}	(26.1)	{3.0×10^{-2}}
105	209	1.48×10^{-7}	3.2×10^{2}	2.36	2.23	1.99	---	{8.87×10^{-6}}	---	{9.5×10^{-3}}
110	240	7.01×10^{-8}	7.8×10^{2}	2.36	2.25	2.00	---	{8.87×10^{-6}}	---	{2.3×10^{-2}}

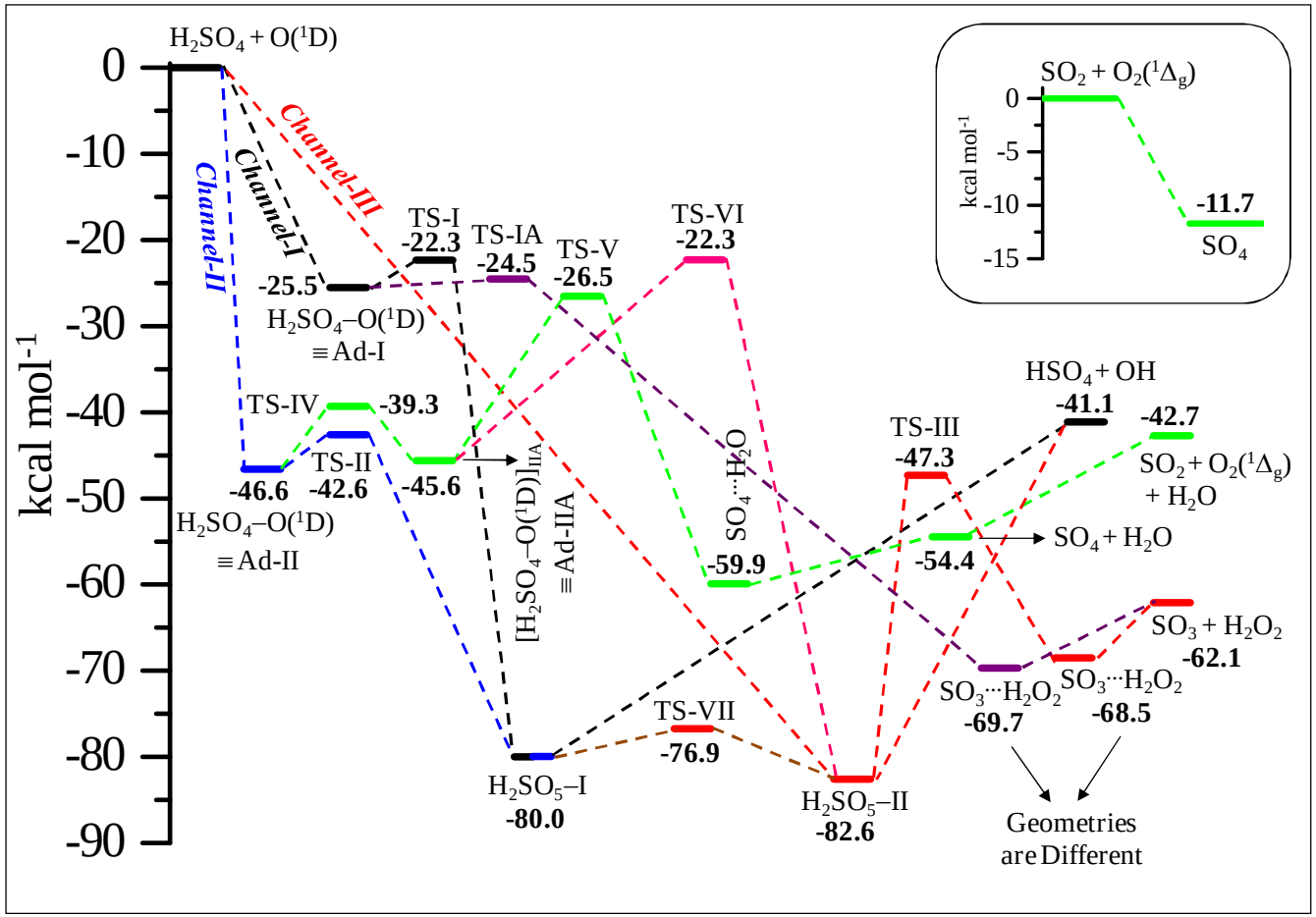

Supplementary Figure 1. Potential energy diagrams with various interconnectivities. The zero point vibrational energy (ZPE) corrected potential energy (kcal mol^{-1}) diagrams with various interconnectivities between three $O(^1D)$−initiated H_2SO_4 insertion reactions via *Channel-I* to *III* have been predicted at the CCSD(T)/aug-cc-pVTZ level. The ZPE corrections in the case of CCSD(T)/aug-cc-pVTZ level of calculations have been done from the M06-2X/aug-cc-pVTZ level predicted ZPE corrections. The optimized geometries of several species involved in the potential energy diagrams have been provided in Supplementary Figure 2. The relative energies of HSO_4 + OH radicals with respect to H_2SO_5 conformers have also been shown in the Figure. The relative energy of $SO_2 + O_2(^1\Delta_g)$ molecules with respect to the SO_4 molecule (singlet) has been shown in the inset of Figure.

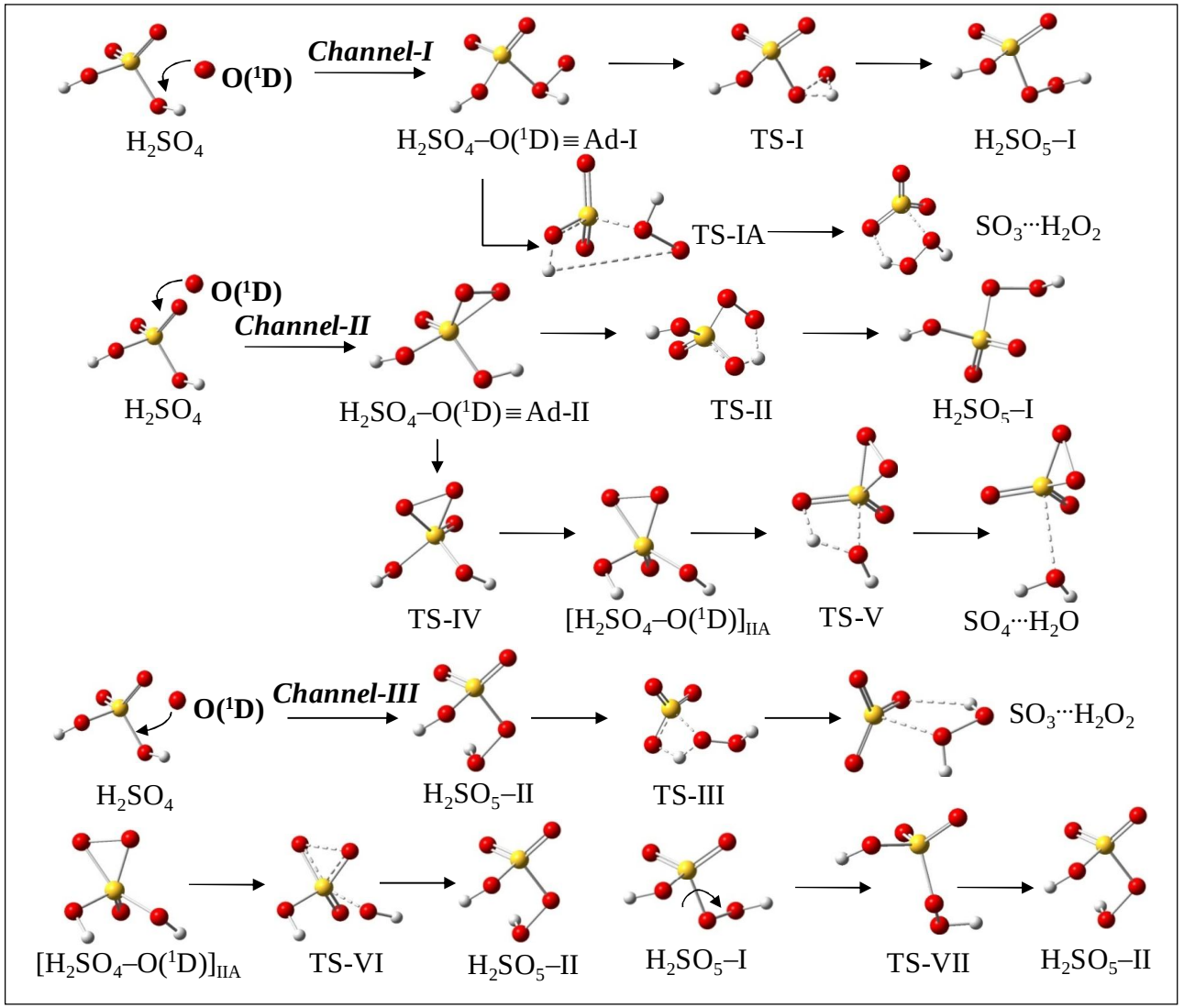

Supplementary Figure 2. The M06-2X/aug-cc-pVTZ level optimized geometries of several species involved in the Supplementary Figure 1. The atoms with yellow, red and whitish-grey colors of various species represent respectively sulfur, oxygen and hydrogen.

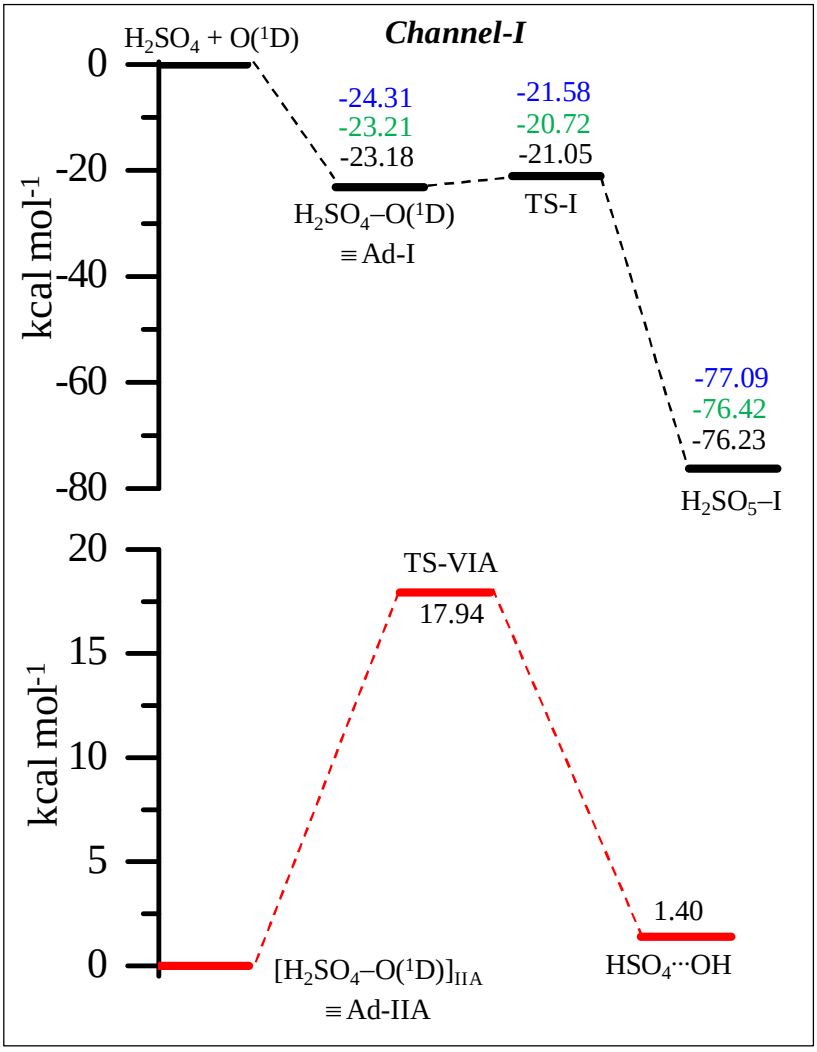

Supplementary Figure 3. Potential energy diagrams at CASPT2 level of calculations. The ZPE corrected CASPT2(12,12)/aug-cc-pVTZ level predicted potential energy (kcal mol^{-1}) profile (black color) for the $O(^1D)$−initiated H_2SO_4 insertion/addition reaction in *Channel-I* via TS-I. The values highlighted by black and green colors have been obtained when the ZPE corrections are made with respect to the predicted ZPE corrections at the CASSCF(12,12)/aug-cc-pVTZ and M062X/aug-cc-pVTZ levels of theories. The potential energy profile for the $O(^1D)$−initiated H_2SO_4 insertion/addition reaction in *Channel-I* via TS-I at the CASPT2(12,12)/aug-cc-pVDZ level has been shown by blue color, and ZPE correction has been done with respect to ZPE correction predicted at the CASSCF(12,12)/aug-cc-pVDZ level of theory.The CASPT2(12,12)/aug-cc-pVTZ level calculated potential energy profile (red) for the unimolecular Ad-IIA→ HSO_4···OH reaction step via TS-VIA has also been shown in the same Figure.

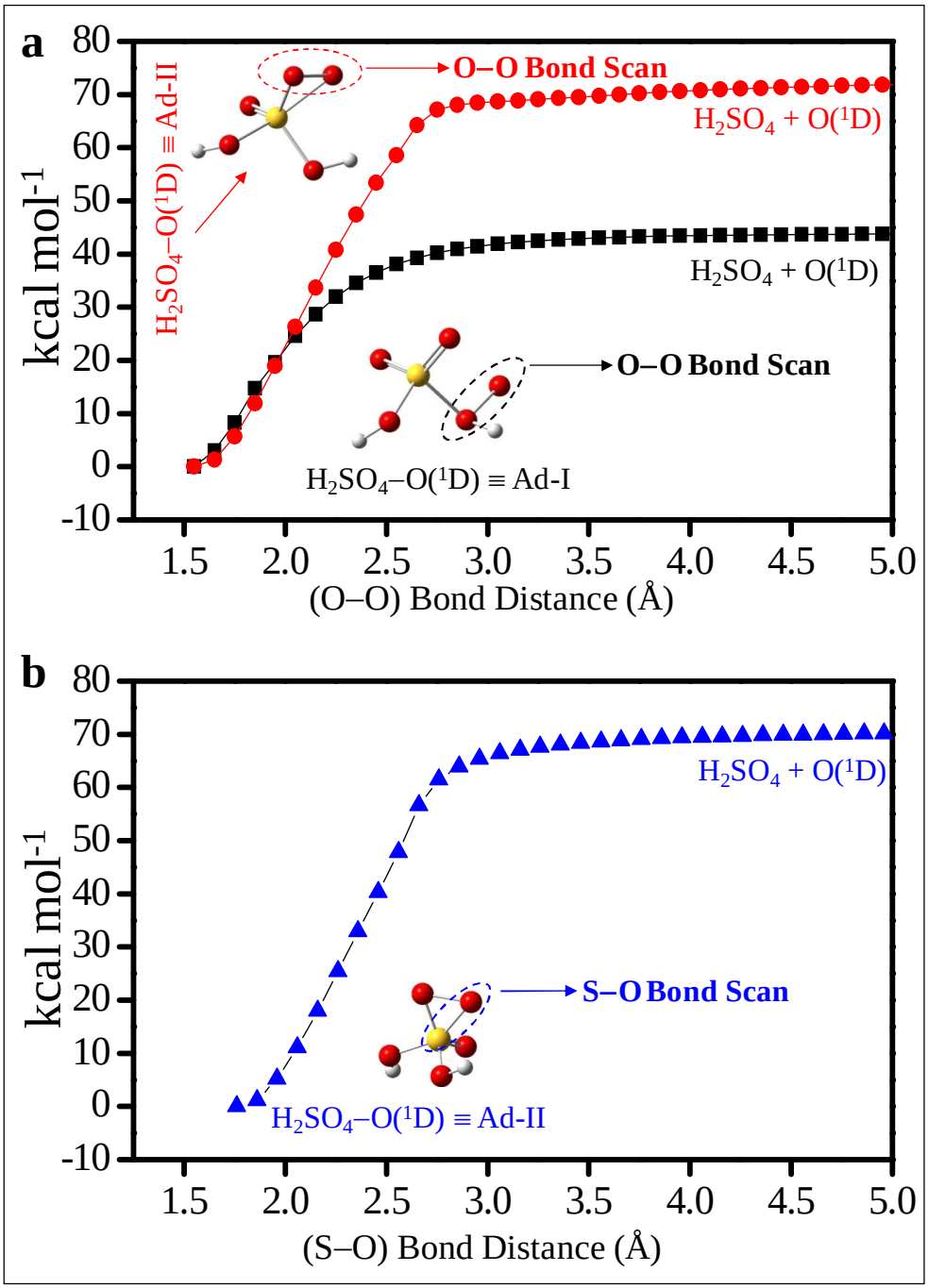

Supplementary Figure 4. One dimensional approximate potential energy curves. The CASPT2(12,12)/aug-cc-pVDZ//CASSCF(12,12)/aug-cc-pVDZ level of calculations have been performed to obtain the approximate potential energy (kcal mol^{-1}) curves along the O–O and S–O bonds of Ad-I and Ad-II through scanning from their equilibrium distances to 5 Å with 0.1 Å step size, as described above in the Supplementary Note-1. **a** O–O bond scan of Ad-I and Ad-II. **b** S–O bond scan of Ad-II.

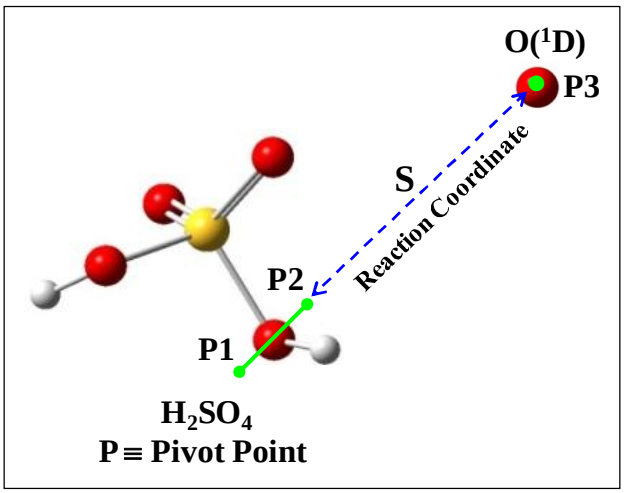

Supplementary Figure 5. Visualization of the configuration of pivot points for the insertion reaction of $O(^1D)$ into the O−H bond of the H_2SO_4 molecule. The P (P1, P2, P3) and S represent respectively the pivot points and reaction coordinate between the pivot points.

Supplementary References:

1. Lee, T. J. & Taylor, P. R. A diagnostic for determining the quality of single-reference electron correlation methods. *Int. J. Quantum Chem.* **23,** 199−207 (1989).

2. Rienstra-Kiracofe, J. C., Allen, W. D. & Schaefer III, H. F. The $C_2H_5 + O_2$ reaction mechanism: high-level ab Initio characterizations. *J. Phys. Chem. A* **104,** 9823−9840 (2000).

3. Thomas, L. H. & Kaltsoyannis, N. An ab initio study of the electronic structure of BCl_2^{3+} and its decomposition pathways. *Phys. Chem. Chem. Phys.* **8,** 1271–1281 (2006).

4. Lambert, N., Kaltsoyannis, N., Price, S. D., Žabka, J. & Herman, Z. Bond-forming reactions of dications with molecules: A computational and experimental study of the mechanisms for the formation of HCF_2^+ from CF_3^{2+} and H_2. *J. Phys. Chem. A* **110,** 2898−2905 (2006).

5. Roehl, C. M., Nizkorodov, S. A., Zhang, H., Blake, G. A. & Wennberg, P. O. Photodissociation of Peroxynitric Acid in the Near-IR. *J. Phys. Chem. A* **106,** 3766–3772 (2002).

6. Stark, H. et al. Overtone dissociation of peroxynitric acid (HO_2NO_2): absorption cross sections and photolysis products. *J. Phys. Chem. A* **112,** 9296−9303 (2008).

7. Indulkar, Y. N., Louie, M. K. & Sinha, A. UV photochemistry of peroxyformic Acid (HC(O)OOH): an experimental and computational study investigating 355 nm photolysis. *J. Phys. Chem. A* **118,** 5939–5949 (2014).

8. Liu, Y.-J., Persson, P. & Lunell, S. Theoretical study of the photodissociation of low lying excited states of hydrogen peroxide *Mol. Phys.* **102,** 2575−2584 (2004).

9. Vaida, V. & Donaldson, D. J. Red-light initiated atmospheric reactions of vibrationally excited molecules. *Phys. Chem. Chem. Phys.* **16,** 827-836 (2014).

10. Hazra, M. K., Matthews, J. & Sinha, A. Influence of initial parent vibrational excitation in promoting two-photon absorption in HOOH and CH_3OOH. *Chem. Phys. Lett.* **512,** 25−29 (2011).

11. Vaghjiani, G. L. & Ravishankara, A. R. Photodissociation of H_2O_2 and CH_3OOH at 248 nm and 298 K: Quantum yields for OH, $O(^3P)$ and $H(^2S)$. *J. Chem. Phys.* **92,** 996−1003 (1990).

12. Matthews, J. Fry, J. L., Roehl, C. M., Wennberg, P. O. & Sinha, A. Vibrational overtone initiated unimolecular dissociation of $HOCH_2OOH$ and $HOCD_2OOH$: evidence for mode selective behavior. *J. Chem. Phys.* **128,** 184306 (2008).

13. Watts, J. D. & Francisco, J. S. Ground and electronically excited states of methyl hydroperoxide: Comparison with hydrogen peroxide. *J. Chem. Phys.* **125,** 104301 (2006).

14. Eisfeld, W. & Francisco, J. S. Excited states and photodissociation of hydroxymethyl hydroperoxide. *J. Chem. Phys.* **128,** 174304 (2008).

15. Kohguchi, H. et al. Collision energy dependence of the $O(^1D) + HCl \rightarrow OH + Cl(^2P)$ reaction studied by crossed beam scattering and quasiclassical trajectory calculations on ab initio potential energy surfaces. *J. Phys. Chem. A* **112,** 818–825 (2008).

16. Aoiz, F. J. et al. The $O(^1D) + H_2$ reaction at 56 meV collision energy: A comparison between quantum mechanical, quasiclassical trajectory, and crossed beam results. *J. Chem. Phys.* **116,** 10692− 10703 (2002).

17. Sayós, R., Oliva, C. & González, M. A theoretical approach to the $O(^1D) + H_2O(X^1A_1)$ reaction: Ab initio potential energy surface and quasiclassical trajectory dynamics study. *J. Chem. Phys.* **113,** 6736− 6747 (2000).

18. Lin, J. J., Shu, J., Lee, Y. T. & Yang. X. Multiple dynamical pathways in the $O(^1D) + CH_4$ reaction: a comprehensive crossed beam study. *J. Chem. Phys.* **113,** 5287− 5301 (2000).

19. Sayós, R. Hernando, J., Puyuelo, M. P., Enríquez, P. A. & González, M. Influence of collision energy on the dynamics of the reaction. $O(^1D) + CH_4(X^1A_1) \rightarrow OH(X^2\Pi) + CH_3(X^1A_2'')$. *Phys. Chem. Chem. Phys.* **4,** 288–294 (2002).

20. Laidler, K. J. *Chemical Kinetics*. (McGraw Hill, New York, 1965).

21. Zheng, J. et al. *POLYRATE, version 2010,* (2010).

22. Zheng, J. et al. *GAUSSRATE, version 2009-A,* (2010).

23. Georgievskii, Y. & Klippenstein, S. J. Variable reaction coordinate transition state theory: analytic results and application to the $C_2H_3+H\rightarrow C_2H_4$ reaction. *J. Chem. Phys.* **118,** 5442–5455 (2003).

24. Georgievskii, Y. & Klippenstein, S. J. Transition state theory for multichannel addition reactions: multifaceted dividing surfaces. *J. Phys. Chem. A* **107,** 9776–9781 (2003).

25. Bao, J. L., Zhang, X. & Truhlar, D. G. Barrierless association of CF_2 and dissociation of C_2F_4 by variational transition-state theory and system-specific quantum rice–ramsperger–kassel theory. *Proc. Natl. Acad. Sci. U. S. A.* **113,** 13606–13611 (2016).

26. Garrett, B. C. & Truhlar, D. G. Generalized transition state theory. classical mechanical theory and applications to collinear reactions of hydrogen molecules. *J. Phys. Chem.* **83,** 1052–1079 (1979).

27. Truhlar, D. G. & Garrett, B. C. Variational transition-state theory. *Acc. Chem. Res.* **13,** 440–448 (1980).

28. Truhlar, D. G., Isaacson, A. D. & Garrett, B. C. Generalized transition state theory in *Theory of Chemical Reaction Dynamics*. M. Baer, Ed (CRC Press, Boca Raton, FL, 1985), Vol. 4, pp. 65-137.

29. Truhlar, D. G., Garrett, B. C. & Klippenstein, S. J. Current status of transition-state theory. *J. Phys. Chem.* **100,** 12771–12800 (1996).

30. Klippenstein, S. J. A bond length reaction coordinate for unimolecular reactions. II. microcanonical and canonical implementations with application to the dissociation of nitrosyl cyanide (NCNO). *J. Chem. Phys.* **94,** 6469–6482 (1991).

31. Klippenstein, S. J., Georgievskii, Y. & Harding, L. B. Predictive theory for the combination kinetics of two alkyl radicals. *Phys. Chem. Chem. Phys.* **8,** 1133–1147 (2006).

32. Page, M. & McIver Jr, J. W. On evaluating the reaction path hamiltonian. *J. Chem. Phys*. **88,** 922-935 (1988).

33. Zheng, J., Zhang, S. & Truhlar, D. G. Density functional study of methyl radical association kinetics. *J. Phys. Chem. A* **112,** 11509-11513 (2008).

34. Miller, J. A. & Klippenstein, S. J. Theoretical considerations in the NH_2 + NO reaction. *J. Phys. Chem. A* **104,** 2061-2069 (2000).

35. Fernández-Ramos, A., Miller, J. A., Klippenstein, S. J. & Truhlar, D. G. Modeling the kinetics of bimolecular reactions. *Chem. Rev*. **106,** 4518−4584 (2006).

36. Phillips, L. F. A priori rate constant for the reaction NH_2 + NO $\rightarrow$ N_2 + H_2O. *Chem. Phys. Lett*. **135,** 269-274 (1987).

37. Lesclaux, R., Khé, P. V., DeZauzier, P. & Soulignac, J. C. Flash photolysis studies of the reaction of NH_2 radicals with NO. *Chem. Phys. Lett*. **35,** 493-497 (1975).

38. Miller, J. A. Theory and modeling in combustion chemistry. *Proc. Combust. Inst*. **26,** 461-480 (1996).

39. Han, D. et al. Theoretical investigation on the mechanisms and kinetics of OH-initiated photooxidation of dimetyl phthalate (DMP) in atmosphere. *Chemosphere* **95,** 50-57 (2014).

40. Raghunath, P. & Lin, M. C. Ab initio chemical kinetics for the ClOO + NO Reaction: Effects of temperature and pressure on product branching formation. *J. Chem. Phys*. **137,** 014315 (2012).

41. Glowacki, D. R., Liang, C-H., Morley, C., Pilling, M. J. & Robertson, S. H. MESMER: an open-source master equation solver for multi-energy well reactions. *J. Phys. Chem. A* **116,** 9545–9560 (2012).

42. Welty, J. R., Wicks, C. E., Wilson, R. E. & Rorrer, G. L. *Fundamentals of Momentum, Heat and Mass Transfer* (Wiley, New York, 2001).

43. Turco, R. P., Hamill, P., Toon, O. B., Whitten, R. C. & King, C. S. A. One-dimensional model describing aerosol formation and evolution in the stratosphere: I. physical processes and mathematical analogs. *J. Atmos. Sci*. **36,** 699–717 (1979).

44. Weisenstein, D. K. et al. A two-dimensional model of sulfur species and aerosol. *J. Geophys. Res.* **102,** 13019−13035 (1997).

45. DeMore, W. B. et al. Chemical kinetics and photochemical data for use in stratospheric modeling, *JPL Publ. No. 97-4* (1997).

46. Brasseur, G. P. & Solomon, S. *Aeronomy of the Middle Atmosphere* (Springer, Netherlands, 2005).

47. Miller, Y., Gerber, R. B. & Vaida, V. Photodissociation yields for vibrationally excited states of sulfuric acid under atmospheric conditions. *Geophys. Res. Lett*. **34,** L16820 (2007).

48. Feierabend, K. J., Havey, D. K., Brown, S. S. & Vaida, V. Experimental absolute intensities of the $4\nu_9$ and $5\nu_9$ O–H stretching overtones of H_2SO_4. *Chem. Phys. Lett*. **420,** 438−442 (2006).

49. Vaida, V., Kjaergaard, H. G., Hintze, P. E. & Donaldson, D. J. Photolysis of sulfuric acid vapor by visible solar radiation. *Science* **299,** 1566−1568 (2003).

50. Burkholder, J. B., Mills, M. & McKeen, S. Upper limit for the UV absorption cross sections of H_2SO_4. *Geophys. Res. Lett*. **27,** 2493−2496 (2000).

51. Lane, J. R. & Kjaergaard, H. G. Calculated electronic transitions in sulfuric acid and implications for its photodissociation in the atmosphere. *J. Phys. Chem. A* **112,** 4958–4964 (2008).

52. Mandal, M., Ghosh, S. & Maiti, B. Dynamics of the $C(^3P)$ + ethylene reaction: a trajectory surface hopping study. *J. Phys. Chem. A* **122,** 3556−3562 (2018).

53. Frisch, M. J. et al. *Gaussian 09, Revision C.01*, (Gaussian, Inc., 2010).

54. Tully, J. C. Molecular dynamics with electronic transitions. *J. Chem. Phys*. **93,** 1061−1071 (1990).

55. Schmidt, M. W. et al. General atomic and molecular electronic structure system. *J. Comput. Chem.* **14,** 1347−1363 (1993).

56. Fedorov, D. G. & Gordon, M. S. A study of the relative importance of one and two-electron contributions to spin–orbit coupling. *J. Chem. Phys.* **112,** 5611−5623 (2000).